Human SKI is a telomere-associated complex involved in DNA-RNA hybrid control and telomere stability.

Emilia Herrera-Moyano*[1,2], Rosa Maria Porreca*[1,2], Lepakshi Ranjha*[1,2], Roser Gonzalez-Franco*[1,2], Eleni Skourti[1,2], Ying Sun[1,2], Emmanouil Stylianakis[1,2], Alex Montoya[3], Holger Kramer[3] and Jean-Baptiste Vannier[1,2#]

1: Telomere Replication & Stability group, Medical Research Council London Institute of Medical Sciences, London, United Kingdom.
2: Institute of Clinical Sciences, Faculty of Medicine, Imperial College London, London, United Kingdom.
3: Biological Mass Spectrometry & Proteomics, MRC-LMS, Hammersmith Hospital Campus, London W12 0NN, UK

*: equal contribution to the work
#: correspondence, requests for materials and Lead Author: j.vannier@lms.mrc.ac.uk

Summary

Super killer (SKI) complex is a well-known cyplasmic 3′ to 5′ mRNA decay complex that functions with the exosome to degrade excessive and aberrant mRNAs. Recently, SKIV2L, the 3′ to 5′ RNA helicase of the human SKI (hSKI) complex was implicated in the degradation of nuclear non-coding RNAs escaping to the cytoplasm. Here, we show that hSKI is also present in the nucleus, on chromatin and in particular at telomeres during the G2 cell cycle phase. hSKI preferentially binds single stranded telomeric DNA and DNA-RNA hybrids, and SKIV2L interacts with telomeric Shelterin factors TRF1, TIN2, TPP1 and POT1. Loss of SKIV2L leads to telomere loss, DNA damage activation and fragility, which we attribute to replication stress caused by the accumulation of telomeric DNA-RNA hybrids. Our results reveal a nuclear function of the hSKI complex and implicate SKIV2L in averting DNA-RNA hybrid-dependent replication stress at human telomeres.

Introduction

To tackle the challenge of aberrant or excessive cytoplasmic and nuclear RNA molecules, cells have evolved different RNA decay pathways. Among these, the nonsense-mediated mRNA decay (NMD) surveillance pathway is involved in the degradation of mRNAs presenting premature translation termination (Isken and Maquat, 2007) and also works as a quality-control system regulating the expression of physiological mRNAs (Alonso, 2005; Hug et al., 2016). Although NMD has largely been investigated for its cytoplasmic functions (Singh et al., 2007), some components of the human NMD core machinery have been identified in the nucleus, where they target several essential biological processes including telomere homeostasis (Azzalin and Lingner, 2006).

Telomeres are transcribed by RNA polymerase II from subtelomeric regions towards the ends of chromosomes into the long non-coding telomeric repeat-containing RNA (TERRA) (Azzalin and Lingner, 2015). TERRA transcription and its association with telomeres is coordinated through the cell cycle to allow for correct post-replication processing of telomeres but also to avoid collisions between DNA replication and transcription (Maicher et al., 2012; Porro et al., 2010). Due to the complementary nature of TERRA to telomeric DNA, R-loops, constituted by the DNA-RNA hybrid and the displaced DNA strand, may form at telomeres and result in telomeric DNA replication stress (Balk et al., 2013; Sagie et al., 2017). TERRA levels vary in a cell-cycle-dependent manner, with levels peaking in G1 phase, continuously decreasing in S phase and reaching the lowest level in S/G2 (Porro et al., 2010), which suggests the presence of a regulatory mechanism. Indeed, the RNA helicase UPF1, involved in the RNA quality control NMD pathway, is associated with chromatin during S phase (Azzalin and Lingner, 2006) and particularly with telomeres *in vivo* (Azzalin et al., 2007). Its activity is essential to ensure replication and telomere length homeostasis, which is proposed to be mediated by the displacement of TERRA from telomeres (Chawla et al., 2011).

In *Saccharomyces cerevisiae*, the cytoplasmic 3′ to 5′ mRNA decay relies on the super killer (SKI) and exosome complexes. The yeast SKI tetramer is composed of

Ski2, Ski3, Ski8 in a ratio of 1:1:2 (corresponding to SKIV2L, TTC37, WDR61 in humans, respectively) (Halbach et al., 2013; Mitchell and Tollervey, 2003; Schmidt et al., 2016). Ski2 possesses 3' to 5' RNA helicase activity that channels the single-stranded RNA into the exosome for further degradation via an interaction with Ski7 (Halbach et al., 2013; Wang et al., 2005). Consistent with the function of its yeast homolog, human SKIV2L has been reported to facilitate cytoplasmic degradation of mRNAs and viral RNA via the exosome and to play a role in RNA interference (Aly et al., 2016; Chen et al., 2001; Orban and Izaurralde, 2005; van Hoof et al., 2002). Recently, the human SKI (hSKI) complex was shown to directly interact with ribosomal complexes and extract mRNA from these complexes *in vitro* (Zinoviev et al., 2020). Indeed, SKIV2L works in a translation surveillance program with the RNA binding protein AVEN, preventing ribosome stalling by eliminating RNA transcripts (Tuck et al., 2020). Its implication in different RNA regulatory pathways and indication that human SKIV2L localises both in the cytoplasm and in the nucleoli (Qu et al., 1998), is suggestive of a possible role for the hSKI complex in nuclear RNA surveillance.

Our data suggest that a fraction of the hSKI complex localises to chromatin and is enriched at telomeres during G2 phase of the cell cycle. Immunoprecipitation of endogenous SKIV2L revealed an interaction with components of the telomere binding complex, Shelterin. Notably, purified hSKI from insect cells not only interacts with RNA but also has a high affinity for DNA and particularly single stranded (ss) telomeric DNA. Strikingly, hSKI binds DNA-RNA hybrids and loss of SKIV2L is associated with increased accumulation of nuclear DNA-RNA hybrids, persistence of C-rich ssDNA and loss of POT1 from telomeres. Our results suggest that hSKI is involved in the removal of DNA-RNA hybrids from telomeres to ensure telomere maintenance. Indeed, human cells deficient for SKIV2L present ATM-dependent DNA damage activation at telomeres and telomere abnormalities including loss and fragility. The latter is supressed by the depletion of TERRA molecules or by over-expressing RNase H1. We conclude that hSKI is recruited to telomeres to prevent DNA-RNA hybrid accumulation to ensure the integrity of telomeres before mitosis.

Results

The human SKI (hSKI) complex binds to telomere and is enriched in G2.

In order to assess the localisation of the human SKI (hSKI) complex within HeLa cells, we firstly employed cell fractionation. The three components of hSKI: SKIV2L, TTC37 and WDR61 were detected in the whole cell lysate and the chromatin-bound fraction, while the soluble fraction only contained SKIV2L (Figure 1A). Because other factors of the NMD pathway have been associated with telomeres in S-phase of the cell cycle (Azzalin and Lingner, 2006; Azzalin et al., 2007), we decided to specifically assess the binding of hSKI components to telomeres and throughout the different phases of the cell cycle. Cells were arrested in G1 with a double thymidine block, released and collected at different time points (Figures S1A and S1B). Telomere binding was examined using Proteomic of Isolated Chromatin segments (PICh) (Dejardin and Kingston, 2009; Porreca et al., 2020). The PICh analysis was conducted using unique peptides identified in each condition and the respective Label-free quantification (LFQ) values. As expected, peptides from the Shelterin factors: TRF2, TRF1, RAP1, TIN2, TPP1 and POT1 were found enriched in the reads obtained with the telomeric probe compared to the scrambled probe, which confirms specificity and success of the experiment (Figure S1C). Interestingly, the three components of the hSKI complex were also found in the telomere probe-derived peptide reads, with SKIV2L and TTC37 significantly enriched during G2 phase (Figure 1B).

To further validate the presence of the hSKI complex at telomeres, we successfully generated and analysed SKIV2L knockdown (shSKIV2L) and control (shCONTROL) HeLa cells (Figure 1C). Notably, the depletion of SKIV2L was accompanied by a decrease in the levels of the other two hSKI components (TTC37 and WDR61) but had no effect on the levels of its paralog, SKIV2L2, which is known to regulate hTR levels (Nguyen et al., 2015; Taylor et al., 2014; Tseng et al., 2015). Therefore, any phenotype described herein upon SKIV2L depletion is SKIV2L2-independent. Using immunofluorescence, we examined the co-localisation of each of the hSKI complex components with TRF2, protein that localises telomeres. All three hSKI components were identified at telomeres in both asynchronous and G2 phase cells (Figure 1D). Notably, the levels of localisation of both SKIV2L and TTC37 at telomeres were significantly increased during G2, when compared to the asynchronous population. Moreover, and in agreement with the western blot data (Figure 1C), we observed the loss of co-localisation of all three hSKI components with TRF2 in asynchronous and G2 synchronised SKIV2L depleted cells (Figures 1D and S1D). Telomeric ChIP-dot

blot confirmed higher levels of SKIV2L at telomeres during G2, which was significantly reduced in SKIV2L-depleted cells (Figure 1E). Interestingly, ChIP analysis also showed that TRF2 binding to telomeres in G2 is affected by the absence of SKIV2L, which suggests a crosstalk between SKIV2L and Shelterin.

To investigate the interactions between these factors, we performed immunoprecipitation experiments using endogenous proteins. Strikingly, we found that SKIV2L interacts with members of the Shelterin complex; specifically, TRF1, TIN2, POT1 and TPP1 (Figure 1F), particularly in G2 phase of the cell cycle. Taken together, these results indicate that hSKI localises to chromatin and to telomeres.

Purified hSKI complex binds DNA and RNA

To shed light on the potential nuclear function of the hSKI complex and understand how it interacts with telomeres, we resorted to the purification of the whole complex followed by *in vitro* biochemical assays. We designed N-terminus MBP-tagged SKIV2L and N-terminus His-Flag tagged TTC37 to purify the whole complex (Figure 2A). Subsequent affinity and size exclusion chromatography were used to achieve purification of the hSKI complex (Figure 2B).

As SKIV2L contains two putative RecA-like domains and interacts with mRNA, we set out to evaluate the binding affinity of purified hSKI complex for various nucleic acids using electrophoretic mobility shift assays (Figure 2C). First, we tested the binding affinity of hSKI complex to ssRNA containing a poly(A) tail, and also ssDNA of similar sequence (ss poly(A) and ss poly(A) DNA, respectively). hSKI exhibited binding to these substrates, especially to ssRNA (Figures 2C and 2D). Since hSKI complex localises to telomeres (Figure 1), we then evaluated the binding affinity of hSKI to various telomeric and non-telomeric RNA and DNA substrates including single stranded RNA and DNA (TERRA, TEL 18 and non-TEL 18), and double stranded RNA and DNA (dsRNA/ dsDNA) (Figure 2C). Strikingly, we found that hSKI favours binding to telomeric ssDNA (TEL18, K_d = 12 nM) as compared to non-telomeric ssDNA (Non-TEL18, K_d = 30 nM) of similar length (Figures 2C and 2D). Binding to ssRNA of telomeric sequence, that mimics TERRA, was also observed (Figure 2C, top part); however, the affinity seemed lower than for telomeric ssDNA (TERRA versus TEL18) (Figures 2C and 2D). Importantly, no binding to blunt ended dsDNA and dsRNA was observed (Figures 2C and 2D). These results show that hSKI can bind single stranded telomeric polynucleotides.

Purified hSKI complex binds telomeric DNA-RNA hybrids with single-stranded 3' end and regulates these structures in vivo.

As hSKI was able to bind both ssDNA and ssRNA, we next tested the complex for its specificity towards various duplex substrates (dsDNA, dsRNA, and hybrids) containing either 3' or 5' overhangs that could mimic telomere structures *in vitro* (Figure 3A and S2A). Consistent with its higher affinity for telomeric ssDNA than ssRNA, hSKI showed a preference for substrates containing telomeric DNA 3' overhangs (3' TEL D:R and 3' TEL D:D) compared to substrates containing RNA 3' overhangs (3' TERRA R:D and 3' ss poly(A) R:R) (Figure 3A, black versus blue lines) and independently of the RNA sequence (3' ss R:R II and 3' ss R:D II; Figure S2A). Additionally, hSKI showed a 2-fold preference for telomeric DNA 3' overhang with complementary RNA (3' TEL D:R; K_d of 12 nM) compared to telomeric dsDNA with 3' overhang (3' TEL D:D; K_d of 24 nM) (Figure 3A, black lines), highlighting the importance of a RNA-DNA junction for hSKI binding. Furthermore, hSKI showed no binding for structures containing 5' overhang (5' TEL D:D and 5' ss R:R), consistent with its 3' to 5' polarity (Figure S2A). All in all, the similar affinity for telomeric ssDNA and 3' DNA overhang substrates suggests that hSKI complex might potentially load itself on ssDNA at telomeres. SKIV2L belongs to the Ski-2 like family of RNA helicases and contains an ATPase domain. Indeed, our purified hSKI complex hydrolyses ATP *in vitro* (Figure S2B), which raises the possibility that hSKI might function on telomere structures (G-overhang or DNA-RNA hybrids) by exerting its enzymatic activity (eg. unwinding/ translocation).

Having established that purified hSKI binds preferentially to telomeric DNA-RNA hybrids, we next investigated whether hSKI regulates DNA-RNA hybrids *in vivo*. Immunofluorescence assays using the S9.6 antibody that recognises DNA-RNA hybrids, showed increased staining in shSKIV2L cells when compared to the shCONTROL. Pre-extracted cells treated with RNase III were used to eliminate possible interference with dsRNAs (Figure 3B). This difference was more pronounced when the signal was analysed after excluding the nucleolar signal, reducing the possibility of being caused by the presence of hybrids in this region (Figure S3A). These results suggest a role for SKIV2L in preventing DNA-RNA hybrid accumulation *in vivo*. Telomeric DNA-RNA hybrids form by hybridisation of TERRA molecules with the C-rich telomeric leading strand (Balk et al., 2013; Pfeiffer

et al., 2013). Given the localisation of hSKI complex to telomeres *in vivo* (Figure 1), we hypothesised that SKIV2L might prevent G-rich TERRA molecules from hybridising with free C-rich telomeric ssDNA. Therefore, we investigated the quantities of telomeric C-rich ssDNA in native conditions and after RNase treatment using DNA dot blot. Indeed, we detected a statistically significant 1.5-fold increase of C-rich telomeric ssDNA levels in SKIV2L-depleted conditions compared to control cells, while G-rich ssDNA remained unchanged (Figure 3C). Next, we speculated that this increase is related to the stabilisation of TERRA molecules with C-rich telomeric ssDNA, in the absence of SKIV2L. In turn, telomere structure would be perturbed and lead to deprotection of the telomeric ss 3' overhang available for POT1. We proceeded with telomeric ChIP-dot blot of POT1 in SKIV2L-proficient and -deficient cells. In agreement with higher levels of SKIV2L and POT1 in G2 (Figure 1), we could detect a statistically significant 4-fold increase of POT1 protein in cells synchronised in G2 compared to the asynchronous cell population. Strikingly, SKIV2L depletion led to a statistically significant decrease of POT1 levels at telomeres in G2, by 5-fold (Figure 3D). Altogether, the results suggest a link between SKIV2L and POT1 in preventing the generation of C-rich telomeric ssDNA and TERRA/hybrid accumulation.

SKIV2L suppresses telomere loss, DNA-RNA hybrid-dependent telomere fragility and DNA damage signalling activation.

Non-scheduled DNA-RNA hybrid accumulation, particularly at telomeres, are considered a driver of DNA replication stress and telomere instability (Arora et al., 2014; Garcia-Muse and Aguilera, 2019; Lee et al., 2018; Petti et al., 2019; Silva et al., 2019). Next, we investigated whether the effects of SKIV2L depletion would also perturb telomere stability. Even though total TERRA levels remain unchanged between control and SKIV2L knockdown cells (Figures S3B and S3C), fragility at telomeres and telomere loss (as assessed by telomere FISH) were increased more than 2.5- and 3-fold, respectively, in SKIV2L-depleted cells (Figures 4A, 4B and S4A). Telomere fragility caused by SKIV2L depletion is slightly more pronounced than in shCONTROL cells treated with a low dose of aphidicolin (used as a positive control), which indicates that SKIV2L is important for the maintenance of telomere integrity (Figure S4A). SKIV2L-depleted cells treated with aphidicolin showed suppression of telomere fragility to background levels, which suggests that the effect

is replication-dependent (Figure S4A). Indeed, aphidicolin-treated cells present a delay in the progression through the S phase of the cell cycle, while SKIV2L knockdown has no effect on the cell cycle profile of HeLa cells (Figure S4B).

Since we identified various telomere abnormalities in SKIV2L knockdown cells, we assessed the potential activation of the DNA damage response caused by SKIV2L depletion. We quantified the activation levels of ATM/CHK2- and ATR/CHK1-dependent DNA damage signalling pathways in the presence or absence of SKIV2L and upon treatment with aphidicolin. Even though no change in pS345 CHK1 phosphorylation levels was detected, we observed an increase in the levels of activated ATM (pS1981 ATM phosphorylation) as well as increased activation of CHK2 downstream of ATM (pT68 phosphorylation) in cells depleted of SKIV2L when compared to control cells. No differences were observed between aphidicolin treated and untreated SKIV2L-deficient cells (Figure S4C).

Interestingly, when the activation of these DNA damage response factors was assessed specifically at telomeres via co-localisation with TRF2 (Figure S4D), a 4-fold increase in ATM activation was detected upon SKIV2L depletion. Hindering DNA replication with aphidicolin treatment in SKIV2L-deficient cells suppressed the telomeric ATM activation, similar to the results obtained for telomere fragility. Furthermore, to measure the levels of telomeric DNA double-strand breaks in these cells, we quantified co-localisation of 53BP1 foci at telomeres (TIFs) (Takai et al., 2003). In both aphidicolin treated and SKIV2L-depleted cells, we observed increased levels of TIFs when compared to control cells (Figure S4D). Therefore, we conclude that telomere fragility and ATM activation are caused by DNA replication stress in SKIV2L-depleted cells, while telomere loss and 53BP1-dependent DNA damage occur independently of DNA replication (Figure S4A and S4D).

Telomere fragility is a marker of DNA replication stress, proposed to result from replisome collision with DNA secondary structures including T-loops, G-quadruplexes or DNA-RNA hybrids (Arora et al., 2014; Sfeir et al., 2009; Vannier et al., 2012; Vannier et al., 2013). Considering that SKIV2L depletion induces an accumulation of DNA-RNA hybrids accompanied by high levels of telomere fragility and loss, we decided to investigate the connection between these two phenotypes. Firstly, we downregulated TERRA by transfecting locked nucleic acid (LNA) gapmers antisense oligonucleotides (ASOs) (Chu et al., 2017), in SKIV2L-depleted cells. We found that telomeric fragility, but not telomere loss, was suppressed after TERRA

downregulation (Figure 4A). Importantly, this indicates that the fragility phenotype is dependent on telomeric RNA. Next, we tested whether telomere fragility is caused by an accumulation of telomeric DNA-RNA hybrids occurring in SKIV2L-depleted cells. We transiently overexpressed RNase H1, which degrades the RNA moiety of DNA-RNA hybrids, in SKIV2L-depleted HeLa cells (Figure 4B). Consistent with the previous experiment, overexpression of RNase H1 lead to a statistically significant reduction in telomere fragility, down to control levels. This suggests that SKIV2L prevents telomere fragility, which is dependent on the accumulation of telomeric DNA-RNA hybrids. Taken together, our results implicate the hSKI complex in safeguarding telomere integrity by maintaining a proper telomere structure and preventing DNA-RNA hybrid-dependent DNA replication stress at human telomeres.

Discussion

SKI is an essential cofactor of the RNA exosome function in the cytoplasm, which ensures mRNA turnover and quality control (Aly et al., 2016; Halbach et al., 2013; Tuck et al., 2020; Wang et al., 2005; Zinoviev et al., 2020). However, and to date, no nuclear function has been ascribed to hSKI complex. In this study, we describe a previously unforeseen function of hSKI in the nucleus and particularly at telomeres, where the complex localises during G2 phase of the cell cycle to prevent telomere instability before mitosis. Strikingly, SKIV2L depletion in HeLa cells reduces the recruitment of TTC37 and WDR61 to telomeres, which suggests a pivotal role for SKIV2L in the regulation of hSKI recruitment to telomeres during G2.

The recruitment of hSKI to telomeres coincides with a time where TERRA levels are at their lowest during late S/G2 phase, just before TERRA levels start to increase at telomeres (Flynn et al., 2011; Porro et al., 2010). TERRAs can pair with the telomeric leading C-rich DNA strand generating DNA-RNA hybrids. In addition to their physiological function to regulate telomere biology (Balk et al., 2013; Chu et al., 2017; Graf et al., 2017), these structures constitute obstacles for the replication fork and perturb genome stability (Crossley et al., 2019; Garcia-Muse and Aguilera, 2019), particularly at telomeres (Arora and Azzalin, 2015; Arora et al., 2014; Sagie et al., 2017). We observed that TERRA levels are not overly affected, but DNA-RNA hybrids accumulate in SKIV2L-depleted cells. Moreover, telomere fragility is supressed upon TERRA downregulation or overexpression of RNase H1 ribonuclease, a well-accepted factor that intervene at telomere hybrids (Arora et al.,

2014; Silva et al., 2019). This indicates a key role for SKIV2L in preventing DNA-RNA hybrid accumulation and telomere instability. This function could be exerted by the hSKI complex alone or in concert with other RNA regulatory factors, including 5' to 3' RNA helicase UPF1, hEST1A or SMG1, all involved in telomere length homeostasis by negatively regulating TERRA association with telomeres (Azzalin et al., 2007; Chawla et al., 2011).

SKIV2L belongs to the superfamily 2 (SF2) of RNA helicases and have two characteristic RecA-like domains, responsible for nucleic acid binding as well as ATP hydrolysis (Fairman-Williams et al., 2010). Similar to yeast SKI, hSKI can also hydrolyse ATP, an activity that is also essential for its mRNA extraction role (Halbach et al., 2013; Zinoviev et al., 2020). Our biochemical analysis shows that the hSKI complex binds RNAs including TERRA, but surprisingly the affinity is much higher for telomeric DNA, and in particular DNA-RNA hybrids with 3' overhang DNA. We propose that hSKI could load itself on telomeric ssDNA and displace the RNA moiety of the DNA-RNA hybrid preventing their accumulation. Importantly, this is supported by LC-MS/MS-pull-down assays of synthesised DNA-RNA hybrids that identified SKIV2L and TTC37 as a binding proteins (Wang et al., 2018).

Given that DNA-RNA hybrid substrates used for binding analysis resemble telomeric 3' G-overhang structure, we cannot completely exclude that hSKI binds 3' ssDNA during S/G2 and assists in the loading of the Shelterin factor POT1 during the RPA-POT1 switch, in cooperation with hnRNPA1 and TERRA (Flynn et al., 2011). Indeed, we observed that the binding of POT1 in G2 is reduced in the absence of SKIV2L, however, there was no ATR/CHK1- activation. This is consistent with efficient hnRNPA1-mediated displacement of RPA from the ssDNA, which is sufficient to prevent ATR activation. However, failure to load POT1 and to restore telomere capping would activate ATM and DNA damage signalling (Hockemeyer et al., 2005; Takai et al., 2003), in agreement with our results.

Hence, all together the above data lead us to propose a model in which hSKI has a central role in preventing telomere instability in human cells (Figure S4C). Firstly, hSKI affinity for telomeric DNA containing DNA-RNA hybrids would facilitate the prevention and resolution of those structures, which, when stabilised at telomeres, hinder DNA replication. This in turn results in increased telomere fragility accompanied by accumulation of telomeric C-rich ssDNA. Secondly, SKIV2L protects telomere ends from DNA damage signalling activation. In summary, this

study provides the first evidence that the human SKI complex, known for its cytoplasmic role in NMD, is also a chromatin factor. In particular, hSKI associates with telomeres and prevents TERRA-mediated DNA replication stress and ensures telomere stability before mitosis.

Acknowledgements

We thank Titia de Lange for providing HeLa1.3 cells, Alexis Barr for U2OS cells, Simon Boulton for 293FT cell line and Petr Cejka for Sf9 insect cells. Special thank you to Simon Boulton for constructive talks.

Vannier lab's work is supported by the London Institute of Medical Sciences (LMS), which receives its core funding from UKRI (MRC) and by an ERC Starter Grant (637798; MetDNASecStr). Roser Gonzalez-Franco received an MRC funded PhD fellowship, Jean-Baptiste Vannier and Lepakshi Ranjha are funded by UKRI (MRC). Emilia Herrera-Moyano, Rosa Maria Porreca, Eleni Skourti are funded by ERC Starter Grant (637798; MetDNASecStr). Manos Stylianakis is funded by an MRC PhD fellowship.

Author contributions

R.G.F and J.B.V designed the project and E.H.M, R.M.P, L.R, R.G.F, E.S and J.B.V wrote the manuscript. Molecular biology experiments were carried by E.H.M, R.M.P, R.G.F, E.S and M.S. Biochemistry was conducted by L.R and Y.S.

A.M and H.K performed mass spectrometry running and primary analysis.

Declaration of interests

The authors declare no conflict of interests.

Figure titles and legends

Figure 1. Human SKI complex binds telomeres and is enriched in G2. (A) WB of a subcellular fractionation assay in asynchronous HeLa cells. α-Tubulin (cytoplasmic) and H3 (chromatin-binding) were used as controls. SKIV2L protein band is indicated with an arrow. (B) Proteomics of isolated chromatin segments (PICh) analysis showing the binding of human SKI complex to telomeres throughout the cell cycle (AS, asynchronous; S, S-phase; G2, G2-phase; M, M-phase). Tables

are listing the number of unique peptides isolated including the fold change values of unique peptides normalised to the asynchronous values and the relative LFQ intensity values. (C) WB of the hSKI complex (SKIV2L, TTC37 and WDR61) and SKIV2L2 in control (shCONTROL) and SKIV2L knockdown (shSKIV2L) cells. β-Actin, loading control. (D) Immunofluorescence showing co-localisation of hSKI with TRF2 (telomeres) in AS and G2-synchronysed cells. Colocalising signals are outlined. The % of hSKI foci colocalising with TRF2 are relative to AS samples. Means +/- SEM from two independent experiments are shown. Student's t test *, $p<0.05$; ***, $p <0.001$; ns, non-significant. Scale bar 15 μm. (E) ChIP-dot blot analysis of TRF2, SKIV2L and TRF1 in AS and G2-synchronysed cells. Telomeric enrichment of proteins relative to shCONTROL ± SEM of two independent replicates are shown. Student's t test *, $p<0.05$; ****, $p <0.0001$. (F) Immunoprecipitation of SKIV2L, Shelterin proteins or IgG (negative control) in AS and G2-synchronysed HeLa cells. See also Figure S1.

Figure 2. Purified human SKI complex binds preferentially telomeric ssDNA. (A) Schematic representation of the hSKI constructs. MBP, Maltose binding protein tag; His, 6x histidine tag; Flag, 3x flag tag. Arrows indicate PreScission protease cleavage sites in the constructs. (B) Coomassie blue stained SDS-PAGE gel showing purified hSKI complex (lane 10) with different fractions of purification. The position of each protein is indicated. PP, PreScission protease. (C) Electrophoretic mobility shift assays showing binding of hSKI complex to different RNA substrates (blue lines) and DNA substrates (black lines). Asterisk indicates radioactive ^{32}P label. hSKI protein amounts are indicated. (D) Quantitation of (C) showing % of nucleic acid binding calculated as protein bound substrate signal relative to free substrate signal. Means +/- SEM are shown (n = 2-4).

Figure 3. hSKI complex binds 3' DNA/RNA overhangs preventing DNA-RNA hybrid accumulation, POT1 loss and increase of C-rich ssDNA. (A) Electrophoretic mobility shift assays showing binding of hSKI complex to different 3' overhang DNA/RNA substrates (blue RNA; black DNA). The substrates were made by annealing two DNA strands (D:D), two RNA strands (R:R) or one DNA with one RNA strand (D:R or R:D). Details are as in Figure 2. (B) S9.6 IF staining in shCONTROL and shSKIV2L HeLa cells upon cytoplasm pre-extraction and

treatment with RNAse III. The averages of S9.6 signal intensity per nucleus (A.U., Arbitrary Units) are represented. Median, first and third quartiles are shown (n=300 cells). Mann-Whitney U test ****, p <0.0001. Scale bar, 10 μm. (C) DNA dot blot analysis in shCONTROL and shSKIV2L cells. Single-stranded (ss) C-rich and ss G-rich telomeric DNA (non-denatured) were detected using Telomeric G-rich or C-rich probes respectively. Alu probe was used as a loading control upon denaturation of the membrane. ssDNA signals were normalised to ALU signal and shCONTROL. Means +/- SEM from three independent experiments are shown. Student's t test *, p<0.05; ns, non-significant. (D) ChIP-dot blot analysis of POT1 in AS and G2-synchronysed cells. Details are as in Figure 1E. See also Figure S2 and S3.

Figure 4. hSKI regulates telomeric DNA-RNA hybrids to prevent telomere damage. (A) Metaphases stained with Tel-Cy3 probe (red) and DAPI (blue) from shCONTROL and shSKIV2L HeLa cells upon transfection with gapmer LNA antisense oligonucleotides (ASO) targeting a scramble (control) or TERRA sequences. Examples of telomere fragility (yellow arrows) and loss (green arrows) are outlined. The % of fragile telomeres and telomere loss per metaphase is depicted. Data from two independent experiments are represented as median +/- first and third quartiles (n>40 metaphases). Student's t test ****, p <0.0001; ns, non-significant. Scale bar, 10 μm. (B) Telomeric FISH from HeLa SKIV2L knockdown cells overexpressing RNase H1 (pRNH1, +RNH1) or not (pControl, -RNH1). The % of fragile telomeres per metaphase is depicted. Medians +/- first and third quartiles are shown (n= 20 metaphases). Student's t test **, p<0.01. Scale bar, 10 μm. WB of HeLa cells transfected with an empty plasmid (pControl) or a plasmid overexpressing the RNase H1 (pRNH1) for 24h. β-Actin, loading control. (C) Model proposing the function of the hSKI complex at telomeres. hSKI prevents the accumulation of DNA-RNA hybrids formed by hybridization of TERRAs with single-stranded DNA (ssDNA) at the C-rich leading strand. See also Figure S4.

STAR Methods

Cell culture and generation of stable cell lines

HeLa1.3 cells referred as "HeLa" across the manuscript (kindly provided by T. de Lange) were previously described (Takai et al., 2010). U2OS were a gift from A. Barr and 293FT from S. Boulton. Human cells were cultured in DMEM medium

supplemented with 10% fetal bovine serum (FBS, Sigma-Aldrich, F2442) and maintained at 37ºC in 5% CO_2. *Spodoptera frugiperda* Sf9 insect cells (kindly provided by P. Cejka) were grown at 27˚C in serum free Insect-XPRESS medium (Lonza, BELN12-730Q).

For the generation of SKIV2L and CONTROL knockdown stable cells, lentiviral particles were produced in 293FT cells using pLKO.1 SKIV2L shRNA construct (Dharmacon, 5'-GTACACTATGATCCTCAACTT-3', RNAi Consortium TRCN0000051816) and pLKO.1 GAPDH shRNA construct (Open biosystems, 5'-CTCATTTCCTGGTATGACA-3') (Porreca et al., 2020), respectively. HeLa1.3 cells were transduced following standard procedures. Selection and clonal population generation was achieved with 1 μg/ml puromycin. Cells expressing the shRNA were maintained in 0.25 μg/ml puromycin-containing media.

DNA plasmids

For the generation of the RNaseH1 overexpression construct, a CMV promoter was subcloned upstream of the *RNASEH1* open reading frame fused to a Flag tag. The original construct bearing the *RNASEH1*-Flag fusion (pLVX Tight>*RNASEH1*-Flag Puro) was kindly provided by K.A. Cimprich (Stork et al., 2016). Briefly, *Xho*I and *Not*I-HF restriction enzymes (NEB, R0146 and R3189 respectively) were used for the digestion of both the abovementioned construct and pLenti CMV DEST V5 (pLX302, Addgene, 25896) to excise the Tight promoter from the former and replace it with the CMV constitutive promoter from the latter using ligation of the products of the digestions. As a result, we obtained the construct: pLVX CMV>*RNASEH1*-Flag Puro. Subsequently, we used the QuikChange Lightning Multi Site-Directed Mutagenesis Kit (Agilent #2105130) according to the manufacturer's instructions in order to add a Kozak sequence upstream of the start codon of *RNASEH1* for enhanced expression levels. The primer used for the site-directed mutagenesis to generate the Kozak site was: Kozak_*RNASEH1*_Fw (5'-GTACAAAAAAGCAGGCTTAGCCACCATGATGGAGACAGAGCGA-3'). The resulting construct, pLVX CMV>(Kozak)*RNASEH1*-Flag Puro (mentioned in brief as pRNH1) was the one that we used to transfect cells to overexpress RNaseH1.

Transfections

For transient plasmid (pRNH1, or, as control, pControl (pLenti CMV Puro DEST, Addgene #17452)) transfection into HeLa1.3 Cell Line Nucleofector kit R (Lonza #VVCA-1001) was used according to the manufacturer's instructions. Briefly, 2.6 million HeLa1.3 cells were transfected with 8 µg of plasmid DNA (in a final volume of 100 µl in Nucleofector solution (82 µl) mixed with supplementary solution (18 µl) supplied in the kit. Nucleofector™ II/2b Device (Lonza #LO AAB-1001) programme A-020 was used. Cells were seeded into 2 x 6 cm dishes for each condition and collected after 24 h for downstream analysis; they were either processed into metaphase spreads and subsequent Q-FISH or lysed for analysis on Western blotting.

For TERRA knockdown previously described TERRA (5′-TAACCCTAACCCTAAC-3') and Scramble (5′-CACGTCTATACACCAC-3′) LNA gapmers were synthesised by Exiqon (Chu et al., 2017). 2 x 10^6 HeLa1.3 cells were seeded in a 10 cm dish and transfected with 100 nM of LNA gapmers using Lipofectamine RNAiMAX (Invitrogen 13778150) in a final volume of 3 ml following the manufacturer's instructions, incubated for 3 h before the replacement of medium and collected after 48 h.

Cell synchronisation and drug treatments

HeLa1.3 cells were treated with 2.5 mM thymidine (Sigma-Aldrich, T1895) for 24 h, then washed and allowed to grow in normal media for 16 h followed by a second incubation with 2.5 mM thymidine for 24 h. Cells were released from the block and collected at the specified time points. S-phase or G2-phase enriched cell populations were released for 4 h and 7 h, respectively. For enrichment of mitotic cells, HeLa1.3 were initially treated with 2.5 mM thymidine for 16 h. After 8 h in fresh media they were incubated with nocodazole 50 ng/mL (Sigma-Aldrich, M1404) for 16 h. Cells were collected with no release period. When indicated, HeLa1.3 cells were treated with 0.2 µM aphidicolin for 20 h or with the same amount of DMSO (untreated control).

FACS analysis

HeLa1.3 cells were incubated with 10 µM of EdU (Thermo Fisher, E10415) for 1 h prior to collection. Then, cell suspensions were fixed with formaldehyde 4% (w/v) in PBS for 15 min with vigorous vortexing to dissociate any remaining cellular clumps;

for the same purpose the cells were passed through a syringe with a 0.5 mm needle tip prior to fixation. The Click-iT EdU Alexa Fluor 647 Flow Cytometry Assay kit (Thermo Fisher, C10634) was then used according to the manufacturer's instructions. We counterstained DNA with 10 µg/ml of Propidium Iodide (PI) (Sigma-Aldrich, P4864). Cell preparations were analysed with a BD LSR II flow cytometer.

Fractionation assay

HeLa1.3 cells were scraped in ice-cold CSK buffer (10 mM PIPES KOH pH 6.8, 100 mM NaCl, 300 mM Sucrose, 1.5 mM MgCl2, 5 mM EDTA, 0.5% Triton, cOmplete, EDTA-free Protease Inhibitor Cocktail 2X (Roche, 11873580001), phosphatase inhibitor (Sigma-Aldrich, P0044), homogenised and incubated on ice for 10 min. The 1/3 was kept as the whole cell extract. The rest of the sample was centrifuged for 3 min at 3000 rpm. The supernatant was collected as the soluble fraction, whilst the pellet was washed once with CSK buffer and resuspended in lysis buffer. This was homogenised with a 0.5 mm needle and incubated at room temperature for 20 min before snap freezing.

Immunoprecipitation

HeLa1.3 cells were scraped on ice with cold phosphate buffer saline (PBS) 1X and spun for 5 min at 1200 rpm. Cells were washed once with PBS 1X and spun again. The pellet was incubated with the same volume of RIPA denaturing lysis buffer (50 mM Tris-HCl pH 7.4, 150 mM NaCl, 1% Triton, 0.5% Sodium Deoxylcholate, 0.1% SDS, 1 mM EDTA, 2X proteinase inhibitors, 1 mM PMSF): PBS 1X (1:1). The lysates were spun at 16000 g following a 30 min rotation at 4°C. The supernatant was pre-cleared with protein A beads (1:1) (Thermo Fisher, 10002D) for 30 min in rotation at 4°C. After centrifugation, 5% of the supernatant was kept as INPUT, while the remaining was incubated for 16 h with 10 µg of the pull-down antibody at 4°C in rotation. For antibody capture, protein A beads (1 volume of the original pellet) were added to the samples followed by an incubation at 4°C for 2 h rotating. After three centrifugation and washing steps with lysis buffer, proteins were eluted from the beads via incubation for 5 min at 95°C in a shaker and supplemented with 50 µl of 2X Laemmli buffer. Removal of beads was achieved via centrifugation. Upon

processing, all samples were snap frozen in dry ice. Samples were denatured and prepared for Western blotting analysis.

Western blotting (WB)

Cells were trypsinised, spun down at 300 g for 5 min, washed in PBS 1X and spun down again at 300 g for 5 min. Cell pellets were subjected to lysis by incubating in lysis buffer with the following composition: NaCl 40 mM, Tris 25 mM, pH 8; $MgCl_2$ 2 mM; SDS 0.05% (w/v), Benzonase 100 units/ml (Sigma-Aldrich, E1014-25KU) and cOmplete, EDTA-free Protease Inhibitor Cocktail 2X for 10 min on ice. Phosphatase inhibitors were added when analysing a phosphorylated protein. The lysates were sheared by being forced through a 25G needle for 10 times and then incubated on ice for 10 min. Protein concentration was determined using the Bio-Rad Protein Assay Dye Reagent Concentrate (Biorad, 500-0006) according to the manufacturer's instructions. Protein lysates were denatured for 5 min at 100°C after addition of Laemmli buffer 4X (50 mM Tris pH 6.8; 100 mM DTT; 2%SDS; 0.1% bromophenol blue (w/v); 10% glycerol (v/v)), separated on NuPAGE 4-12% Bis-Tris gels and transferred onto a nitrocellulose membrane (Amersham Protran 0.2 µm, GE10600001). The membrane was blocked using non-fat milk 5% (w/v) in PBS-T (PBS 1X; 0.1% Tween-20) (v/v) and subsequently incubated overnight at 4°C with the primary antibody: anti-RNAseH1 (1/500, final concentration 0.2 µg/ml, Abnova, H00246243-M01), anti-β-actin (1/5000, Abcam, ab8226), anti-ATR (1/500, Bethyl A300-138A), anti-CHK1 (1/500, Sigma-Aldrich, C9358), anti-CHK1 pS345 (1/500, Cell signaling, 2348), anti-ATM (1/500, Sigma-Aldrich, A1106), anti-ATM S1981 (1/500, Cell signaling 4526), CHK2 (1/500, Millipore, 05-649), anti-CHK2 pT68 (1/500, Cell signaling, 2661), anti-H3 (1/1000, Abcam, ab10799), anti-SKIV2L (1/1000, Proteintech group, 11462-1-AP), anti-TTC37 (1/500, Novus Biologicals, NBP1-93640), anti-WDR61 (1/500, Sigma-Aldrich, SAB1401852), anti-α-Tubulin (1/1000, Sigma-Aldrich, T6199), anti-TRF2 (1/2000, Novus Biologicals, NB110-57130), anti-RAP1 (1/500, Bethyl, A300-306A), anti-TRF1 (1/500, Abcam, ab66223), anti-TIN2 (1/1000, Sigma-Aldrich, SAB4200108), anti-POT1 (1/500, Abcam, ab124784), anti-TPP1 (1/1000, Sigma-Aldrich, WH00001200M1), diluted in non-fat milk or BSA 5% (w/v) in PBS-T. Subsequently, the membrane was washed 3 x 10 min in PBS-T. Following incubations with HRP-conjugated secondary antibody (anti-mouse and anti-rabbit, Dako, P0447 and P0217) in non-fat milk 5% (w/v) in PBS-T

and 3 x 10 min washes in PBS-T, the signal was visualized using ECL Western blotting reagents (Sigma-Aldrich, RPN2106) and X-ray film exposure (Amersham Hyperfilm ECL Sigma-Aldrich, GE28-9068-35).

Immunofluorescence (IF)

Cells were grown on 4-well culture slides, pre-extracted for 5 min with permeabilisation buffer (50 mM NaCl, 3 mM MgCl2, 20 mM Tris pH 8, 0.5% Triton X-100, 300 mM sucrose), fixed for 15 min in fixative solution (formaldehyde 4% (w/v) / sucrose 2% (w/v)) and permeabilised for another 10 min. Slides were incubated for 30 min with the blocking buffer (10% goat or donkey serum (Stratech Scientific Ltd) in 1X PBS) at 37°C. Then, the primary antibody (anti-SKIV2L, Proteintech group, 11462-1-AP, 1:1000, anti-TTC37, Novus Biologicals, NBP1-93640, 1:500, anti-WDR61, Sigma-Aldrich, SAB1401852, 1:750 or anti-TRF2, Millipore, 05-521, 1:500) was added in blocking buffer and incubated for 1 hour at 37°C. After 3 x 3 min washes with 1X PBS, the secondary antibody (1/400 in blocking buffer, goat anti-rabbit Alexa 594 antibody, Thermo Fisher, A-11037 or donkey anti-mouse Alexa 488 antibody, Thermo Fisher, R37114) was added in blocking buffer for 30 min at 37°C, followed by 3 x 3 min washes with PBS 1X. Finally, mounting media containing DAPI (Prolong gold antifade mountant with DAPI, Invitrogen, P36931) was used to counterstain DNA. For cell cycle study, cells were seeded at a 40% confluence in 4-well slides. After the appropriate synchronisation protocol, cells were incubated for 1 h with 10 µM of EdU before collection. No pre-extraction was performed. Furthermore, for collection of mitotic enriched populations, cells were fixed with 2X fixative solution in media for 15 min to prevent excessive detachment of cells. Afterwards, the Click-iT Edu Alexa Fluor 647 Imaging Kit (Thermo Fisher, C10640) was employed to label DNA synthesis following the manufacturer's indications. Then, a regular immunofluorescence was performed. S9.6 IF was performed as previously described (Barroso et al., 2019; Garcia-Rubio et al., 2018) with minor modifications. Briefly, cells were pre-extracted, fixed and permeabilised as described above. Before the immunostaining, a treatment with Ambion RNase III (1.2 U, ThermoFisher, AM2290) in order to remove dsRNAs that could interfere with the staining for 30 min at 37°C was performed. Cells were blocked for 3 h in blocking buffer (BSA 2% (w/v) in PBS), incubated with the mouse anti-DNA-RNA hybrid S9.6 antibody (1/500, Kerafast ENH001) in blocking buffer overnight at 4ºC followed by 3 washes with PBS

and detection using Alexa Fluor 594 goat anti-mouse secondary antibody (1:800 in blocking buffer) for 1 h at 37°C. Slides were imaged using an Zeiss microscope using Carl Zeiss software. For S9.6 signal quantification in the nucleus excluding the nucleolus signal, a mask using the strong signal in the nucleolus was created and this region was excluded from the analysis.

Quantitative-FISH analysis (Q-FISH)

For metaphase preparation, HeLa1.3 cells were incubated for 1 h with colcemid 10 ng/ml (Roche, 10295892001). Subsequently, cells were collected and incubated for 15 min at 37°C in hypotonic buffer (75 mM KCl: 8 g/L NaCitrate: ddH_2O, 1:1:1). Fixation was performed with freshly prepared fixative (ethanol: glacial acetic acid (3:1)) followed by three washes using the same fixative. Finally, metaphase suspensions were dropped on previously humidified glass slides from a distance of at least 1 m. Slides were covered and allowed to dry overnight at room temperature. Q-FISH was performed as previously described (Ourliac-Garnier and Londono-Vallejo, 2011). Briefly, metaphase spreads were fixed in formaldehyde 4% (w/v) for 2 min, washed 3 x 5 min in PBS 1X, treated with pepsin (1 mg/ml in 0.05 M citric acid pH 2) for 10 min at 37°C, post-fixed for 2 min, washed and incubated in increasing ethanol concentration baths (70%, 80%, 90%, 100%). Each slide was then covered with hybridising solution containing Cy3-O-O-$(CCCTAA)_3$ probe (PNA bio) in formamide 70% (v/v), 10 mM Tris pH 7.4 and 1% (v/v) blocking reagent (Roche, 11096176001). This step was followed by denaturation for 3 min at 80°C on a heat block. Hybridisation was performed for 2 h at room temperature. Slides were washed 2 x 15 min in formamide 70% (v/v) in 20 mM Tris pH 7.4, followed by 3 x 5 min washes in 50 mM Tris pH 7.4, 150 mM NaCl, Tween-20 0.05% (v/v), dehydrated in successive ethanol baths and air-dried. Slides were mounted in antifade reagent containing DAPI and images were captured with Zeiss microscope using Carl Zeiss software. Telomeric signals were quantified using the ImageJ software (Fiji).

PICh and mass spectrometry analysis

PICh experiments were conducted as previously described (Dejardin and Kingston, 2009; Porreca et al., 2020) with minor modifications on the sample processing:

Protein samples were processed using the Filter Aided Sample Preparation (FASP) protocol (Wiśniewski et al., 2009). Briefly, samples were loaded onto 30 kDa

centrifugal concentrators (Millipore, MRCF0R030) and buffer exchange was carried out by centrifugation on a bench top centrifuge (15min, 12,000g). Multiple buffer exchanges were performed sequentially with UA buffer (8M urea in 100mM Tris pH 8.5, 3x200□l), reduction with 10mM DTT in UA buffer (30min, 40°C) and alkylation with 50mM chloroacetamide in UA buffer (20min, 25°C). This was followed by buffer exchange into UA buffer (3x100□l) and 50mM ammonium bicarbonate (3x100□l). Digestion was carried out with mass spectrometry grade trypsin (Promega, V5280) using 1□g protease per digest (18h, 37°C). Tryptic peptides were collected by centrifugation into a fresh collection tube (10min, 12,000g) and washing of the concentrator with 0.5M sodium chloride (50□l, 10min, 12,000g) for maximal recovery. Following acidification with 1% trifluoroacetic acid (TFA) to a final concentration of 0.2%, collected protein digests were desalted using Glygen C18 spin tips (Glygen Corp, TT2C18.96) and peptides eluted with 60% acetonitrile, 0.1% formic acid (FA). Eluents were then dried using vacuum centrifugation.

Liquid chromatography-tandem mass spectrometry (LC-MS/MS) analysis

Dried tryptic digests were redissolved in 0.1% TFA by shaking (1200rpm) for 30min and sonication on an ultrasonic water bath for 10min, followed by centrifugation (13,000 rpm, 5°C) for 10min. LC-MS/MS analysis was carried out in technical duplicates and separation was performed using an Ultimate 3000 RSLC nano liquid chromatography system (Thermo Scientific) coupled to a Q-Exactive mass spectrometer (Thermo Scientific) via an EASY spray source (Thermo Scientific). For LC-MS/MS analysis re-dissolved protein digests were injected and loaded onto a trap column (Acclaim PepMap 100 C18, 100µm × 2cm) for desalting and concentration at 8µL/min in 2% acetonitrile, 0.1% TFA. Peptides were then eluted on-line to an analytical column (Acclaim Pepmap RSLC C18, 75µm × 50cm) at a flow rate of 250nL/min. Peptides were separated using a 120-minute gradient, 4-25% of buffer B for 90 minutes followed by 25-45% buffer B for another 30 minutes (composition of buffer B – 80% acetonitrile, 0.1% FA) and subsequent column conditioning and equilibration. Eluted peptides were analysed by the mass spectrometer operating in positive polarity using a data-dependent acquisition mode. Ions for fragmentation were determined from an initial MS1 survey scan at 70,000 resolution, followed by HCD (Higher Energy Collision Induced Dissociation) of the top 12 most abundant ions at 17,500 resolution. MS1 and MS2 scan AGC targets

were set to 3e6 and 5e4 for maximum injection times of 50ms and 50ms respectively. A survey scan m/z range of 400 – 1800 was used, normalised collision energy set to 27%, charge exclusion enabled with unassigned and +1 charge states rejected and a minimal AGC target of 1e3.

Raw data processing

Data was processed using the MaxQuant software platform (v1.5.8.3), with database searches carried out by the in-built Andromeda search engine against the Swissprot H.sapiens database (version 20170202, number of entries: 20,183). A reverse decoy search approach was used at a 1% false discovery rate (FDR) for both peptide spectrum matches and protein groups. Search parameters included: maximum missed cleavages set to 2, fixed modification of cysteine carbamidomethylation and variable modifications of methionine oxidation, protein N-terminal acetylation, asparagine deamidation as well as glutamine to pyro-glutamate. Label-free quantification was enabled with an LFQ minimum ratio count of 2. 'Match between runs' function was used with match and alignment time limits of 1 and 20 minutes respectively.

Northern blot

RNA extraction was carried out using RNeasy Mini Kit (Qiagen, 74104) and DNA contaminants were eliminated by in column treatment with DNAse A (Qiagen, 79254) according to the manufacturer instructions. RNA (10 µg) was denatured for 10 min at 65°C in sample buffer (formamide 50% (v/v), 2.2 M formaldehyde, 1X MOPS) followed by incubation on ice for 5 min. 10X Dye buffer (glycerol 50% (v/v), Bromophenol Blue 0.3% (w/v), 4 mg/ml ethidium bromide) was added to each sample and they were run on a formaldehyde agarose gel (agarose 0.8% (w/v), formaldehyde 6.5% (v/v) in 1X MOPS) at 5 V/cm in 1X MOPS buffer (0.2M MOPS, 50 mM NaOAc, 10 mM EDTA, RNAse-free water). The gel was rinsed twice in water, washed 5 min with denaturation solution (1.5 M NaCl, 0.05 M NaOH), followed by three more washes with 20X SSC before transferring the RNA on an Amersham Hybond N+ membrane (GE Healthcare, RPN303B) overnight using a neutral transfer in 20X SSC. The membrane was UV-crosslinked (Stratalinker, 200 J/cm^2 UV) and baked for 45 min at 80 °C. The membrane was neutralised by washing twice with 2X SSC and prehybridised for 1 h at 42°C with hybridisation buffer (6X SSC, 0.1% SDS,

1% non-fat milk). Hybridisation with a pre-boiled DIG labelled telomeric probe (1:5000, $(CCCTAA)_3$) was performed overnight at 42°C. The probe was prepared using 3' end labelling kit (Roche, 03353575910) according to the manufacturer's instructions and diluted in hybridisation buffer (6X SSC, 0.1% SDS, 1% milk). The membrane was then washed 2 x 5 min with pre-warmed 2X SSC/0.1% SDS and 1 x 2 min with pre-warmed 0.2X SSC/ 0.1% SDS, then submerged in 2X SSC for 5 min and washed in Tween-20 in maleic acid 0.3% (v/v) for 5 min. Signal was detected using the anti-DIG-alkaline phosphatase antibodies (1:20000, Roche, 11093274910) and CDP-Star (Roche, 11685627001) following the manufacturer's instructions. Images were captured using the Amersham Imager 680 (GE Healthcare) and analysed using the Image Studio Lite software.

RNA dot blot

RNA (5 µg) was incubated in 0.2 M NaOH, denatured at 65°C for 10 min and incubated on ice for 5 min. Finally, RNA was spotted onto a positively charged Amersham Hybond N+ membrane (GE Healthcare, RPN303B) using a dot-blot apparatus. Membranes were UV-crosslinked (Stratalinker, 200 J/cm^2 UV), heated for 30 min at 80°C and hybridised overnight at 42°C with the following digoxigenin (DIG)-labeled probes: telomeric C-rich oligonucleotide $TAA(CCCTAA)_4$; telomeric G-rich probe $ATT(GGGATT)_4$ and 18s rRNA probe CCATCCAATCGGTAGTAGCG. The probes were prepared and the signal was detected as described earlier (see Northern blot section). 18s rRNA signal was used for normalisation.

Chromatin Immunoprecipitation (ChIP)

Chromatin preparation and ChIP experiments were performed as previously described (Porreca et al., 2018) with the following modifications: Chromatin (50 µg) was diluted in 1 ml final volume of ChIP dilution buffer (20 mM Tris-HCl pH 8, 150 mM KCl, 2 mM EDTA pH 8, 1% Triton X-100, 0.1% SDS), pre-cleared for 2 h with Protein A Dynabeads (Invitrogen, 10001D), followed by overnight incubation with 5 µg of antibody (listed in Key Resources Table).

ssDNA dot blot

Cells were washed with PBS 1X, lysed with Hirt buffer (10 mM Tris pH 8, 100 mM NaCl, 10 mM EDTA, 0.5% SDS) with addition of 200µg/ml of RNase A and incubated at 37°C for 1 hour. The whole cell extracts were then incubated overnight with 200 µg Proteinase K (Sigma-Aldrich, P4850) at 55°C. Equal volume of Phenol/ Chloroform/ Isoamyl Alcohol (Invitrogen) was added to the samples, followed by rotation on a wheel for 10 minutes. Samples were spun for 10 minutes at 3000 rpm before performing a second extraction with equal volume of chloroform:isoamyl alcohol (Sigma). 1/10 volumes of 3M NaAc and 2.5 volumes of 100% EtOH were added to each sample. After precipitation, DNA was washed with 70% EtOH before resuspension in ddH_2O overnight. DNA (5 µg) was digested with 50 units *HinfI* (NEB, R0155L) and 50 units *RsaI* (NEB, R0167L) overnight at 37°C. The next day, an additional 10 units of each enzyme were added for a further 2 h incubation at 37°C. 1µg of DNA was used for DNA dot blot experiments. DNA was spotted under native conditions onto an Amersham Hybond- N+ membrane using a dot-blot apparatus and membranes were UV-crosslinked (Stratalinker, 200 J/cm^2 UV). Hybridisation and detection of membranes were carried out as described earlier (see Northern blot section). After stripping the membranes, a further denaturation step was carried out for 20minutes at RT using a solution containing 1.5□M NaCl, 0.5□M NaOH, before proceeding with hybridisation with ALU probe (GGCCGGGCGCGGTGGCTCACGCCTGTAATCCCAGCA).

Preparation of hSKI expression constructs

The SKIV2L, TTC37 and WDR61 genes were synthesised and cloned using standard procedures into pFastbac1 vectors by GenScript with the addition of 6x histidine tag and 3x flag tag before the TTC37 gene creating pFB-SKIV2L, pFB-His-Flag-TTC37 and pFB-WDR61 plasmids respectively. All three genes were codon-optimised for expression in insect cells. The pFB-SKIV2L plasmid was further modified by adding a maltose binding protein tag (MBP) before the SKIV2L gene giving rise to the pFB-MBP-SKIV2L plasmid. All plasmids contained a PreScission protease cleavage site between the tags and the gene to enable cleavage of the tags post-purification. The cloned genes were expressed using bac-to-bac baculovirus expression system in *Spodoptera frugiperda* Sf9 insect cells. Baculovirus particles were produced and the cells were infected with optimal ratios of all three

viruses. After 52 h, the cells were collected, washed with PBS and stored at -80°C until purification.

Purification of hSKI complex

The frozen cell pellet was resuspended in 3 volumes of lysis buffer consisting of 50 mM Hepes-KOH pH 7.6, 1 mM DTT, 1 mM EDTA, 1:400 protease inhibitor cocktail (P8340, Sigma-Aldrich), 1 mM PMSF and 30 µg/ml Leupeptine for 20 min at 4°C with gentle agitation. Then, glycerol (final concentration 16% (v/v)) and NaCl (final concentration 325 mM) were added and the suspension was stirred slowly for 30 min. The suspension was centrifuged at 48000 g for 30 min to obtain the soluble extract. Next, the clarified extract was incubated with pre-equilibrated amylose resin (NEB, E8021S) for 60 min. The protein bound amylose resin was washed with MBP wash buffer containing 50 mM Hepes-KOH pH 7.6, 2 mM β-mercaptoethanol, 250 mM NaCl, 10% glycerol, 1 mM PMSF and 10 µg/ml Leupeptine followed by elution with MBP wash buffer supplemented with 10 mM Maltose. The MBP eluate was then incubated with pre-equilibrated nickel-nitriloacetic acid resin (Ni-NTA agarose, Qiagen, 30210) for 60 min in the presence of 20 mM imidazole. The Ni-NTA resin was washed with Ni-NTA wash buffer containing 50 mM Hepes-KOH pH 7.6, 2 mM β-mercaptoethanol, 150 mM NaCl, 10% glycerol, 0.5 mM PMSF, 40 mM imidazole and eluted with Ni-NTA wash buffer containing 400 mM imidazole. The Ni-NTA eluate was incubated overnight with PreScission protease to cleave the tags. The cleaved eluate was concentrated using a centrifugal filter (50 kDa cut-off, Amicon, UFC905024) and subsequently loaded onto a Superose 6 Increase 10/300 GL column (GE Healthcare, GE29-0915-96). The peak fraction containing recombinant hSKI complex was collected, sub-aliquoted, snap frozen and stored at -80°C until use.

Preparation of DNA/RNA substrates

The sequences of all oligonucleotides are listed in the Key Resources Table. The RNA and DNA oligonucleotides were synthesised and PAGE purified by Sigma-Aldrich. The oligonucleotides were labelled with radioactive ^{32}P at their 5' end by T4 polynucleotide kinase (NEB). The labelled oligo was annealed to the complementary non-labelled oligo in a 1:2 ratio in polynucleotide kinase buffer, heated to 95°C for 5 min followed by cooling overnight. The ssDNA substrates used were TEL18, ss

poly(A) DNA, Non-TEL18 and the ssRNA substrates were TERRA and ss poly(A). The DNA duplex substrates included dsDNA (TEL30 and CTEL30), 5' TEL - D:D (TEL30 and 5'CTEL20), 3' TEL - D:D (TEL30 and 3'CTEL20). The RNA duplex substrates were dsRNA (ss27 and Css27), 5' ss - R:R (5'ss27 and 5'Css17), 3' ss poly(A) - R:R (ss27 and Css17) and 3' ss - R:R II (5'ss27 and Css17). The DNA-RNA hybrid substrates used were 3' TEL - D:R (TEL30 and 3'CTEL20 RNA), 3' TERRA - R:D (TERRA and 5'CTEL20) and 3' ss - R:D II (5'ss27 and Css17 DNA).

Nucleic acid binding assay

The electrophoretic mobility shift assay (EMSA) was carried out in a total reaction of 15 µl in a buffer containing 25 mM Hepes-KOH pH 7.6, 2 mM magnesium acetate, 50 mM NaCl, 1 mM DTT, 0.1 mg/ml BSA, 1 nM DNA/RNA substrate (in molecules) and indicated amounts of hSKI protein complex. The reactions were assembled on ice, incubated at 37°C for 30 min and the products were separated on an agarose gel 0.7% (w/v) at 100 V for 60 min at 4°C. The gel was dried on Hybond-XL paper (GE Healthcare, RPN1520S) in a gel dryer (Biorad), exposed to phosphor screen (GE Healthcare, 28956474) and scanned on FLA-5100 (Fujifilm). The gels were quantitated using Imagequant software (GE Healthcare).

ATP hydrolysis assay

The ATP hydrolysis reaction (10 µl) contained 20 mM Tris-HCl pH 7.5, 4 mM magnesium acetate, 1 mM DTT, 0.5 M ATP and 3 µCi radioactive [γ^{32}P] ATP. The reaction was initiated by adding indicated amounts of hSKI protein complex, incubated for 3.5 h at 37°C before stopping the reaction with 50 mM EDTA. 1 µl of each reaction was spotted on Thin Layer Chromatography plates (TLC plates, PEI cellulose, Merck, 105579). The plates were dried and released radioactive phosphate (Pi) was separated from ATP by chromatography in a solution containing 0.15 M lithium chloride and 0.15 M formic acid. The plates were again dried before exposing to phosphor screens. The screens were scanned using FLA-5100 (Fujifilm). The free 'Pi' signal was quantitated using image J (Fiji).

Statistical analysis

Statistical analysis was performed using GraphPad Prism. Error bars, statistical methods and n, are described in figure legends. Figures were prepared using Adobe Illustrator.

Supplemental Information titles and legends

Figure S1. Synchronisation of HeLa cells at different stages of the cell cycle.

(A) FACS analysis of asynchronous (black) or synchronised (coloured) HeLa cells using double thymidine block. Cells were released from the block and collected every hour (for 8h) for FACS as specified (top panel). FACS analysis of asynchronous (black) and nocodazole blocked (blue) HeLa cells after an 8h release from thymidine arrest (bottom panel). (B) Representative images of Cyclin A immunofluorescence (S-G2 phases) and EdU click-it reaction (S phase) in asynchronous HeLa cells upon incubation with EdU for 1h (top panel). Discrimination between G1 and M phases was based on DAPI signal. Scale bar, 15 μm. Quantification of IF images from asynchronous, synchronised in S phase (4h release), in G2 (7h release) and in prometaphase (after 16h nocodazole block) HeLa cells (bottom panel). Total number of quantified nuclei per condition (N) and the percentage of cells in each cell cycle phase is indicated. (C) Proteomics of isolated chromatin segments (PICh) analysis showing the binding of Shelterin proteins throughout the cell cycle (AS; S; G2; M). Tables are listing the number of unique peptides isolated including the fold change values of unique peptides normalised to the asynchronous values (left panel) and the relative LFQ intensity values identified by PICh (right panel). (D) Representative images of immunofluorescence showing co-localisation of hSKI with TRF2 (telomeres) in asynchronous control (shCONTROL) and SKIV2L-depleted (shSKIV2L) cells. Details of colocalising or non-colocalising signals are outlined.

Figure S2. hSKI complex binds 3'overhangs and hydrolyses ATP.

(A) Electrophoretic mobility shift assays showing binding of hSKI complex to different 3' and 5' overhang RNA/DNA substrates. The substrates were made by annealing two DNA strands (D:D), two RNA strands (R:R) or one RNA with one DNA strand

(R:D). The sequences of these substrates are different from Figure 3A (see key resources table). Asterisk indicates radioactive ^{32}P label. hSKI protein amounts are as indicated (nM). Quantitation of experiments in right panel showing % of nucleic acid binding calculated as protein bound substrate signal relative to free substrate signal. Data are represented as mean +/- SEM (n = 2). (B) Representative image of ATP hydrolysis assay by human SKI complex (left panel). Quantitation of two independent experiments showing ATPase activity of hSKI complex (right panel). The % of ATP hydrolysed is calculated as the amount of hydrolysed phosphate released (Pi) relative to ATP. Data are represented as mean +/- SEM.

Figure S3. Depletion of SKIV2L increases DNA-RNA hybrid levels without affecting total TERRA amounts.

(A) Representative images of S9.6 IF staining in control and SKIV2L-depleted HeLa cells upon cytoplasm pre-extraction and treatment with RNAse III. Dashed lines outlining the nuclei and nucleoli edges are depicted. Nucleolar areas are observed as regions with intense S9.6 signal. Violin plots are representing the average S9.6 signal intensity per nucleus excluding the nucleolar signal (A.U., Arbitrary Units). Median is underlined in red, while first and third quartiles are shown as grey dotted lines (n=300 cells). Mann-Whitney U test ****, $p < 0.0001$. Scale bar, 10 µm. (B) RNA dot blot analysis in shCONTROL and shSKIV2L HeLa cells untreated or treated with aphidicolin (APH). Half of each sample was treated with Ribonuclease A (+ RNase A) before spotting to control for DNA contamination. The blot was revealed with DIG-Telomeric C-rich, Telomeric G-rich (negative control) or 18S rRNA (loading control) probes. TERRA signals were normalized to 18S rRNA signals, relative to shCONTROL untreated. Data are represented as mean +/- SEM from two experiments. RNA from U2OS cells was used as a positive control. (C) TERRA detection by Northern blotting in shCONTROL and shSKIV2L HeLa cells. DIG-Tel C-rich probe was used to detect TERRA. Ethidium bromide staining of the 28S rRNA was used as loading control. *, unspecific band corresponding to the 18S rRNA. Relative RNA signals are depicted at the bottom of each lane of the gel.

Figure S4. SKIV2L prevents telomere fragility, loss and DNA damage signalling activation. (A) Telomere FISH in shCONTROL and shSKIV2L HeLa cells.

Representative enlargements depicting telomere fragility (yellow arrows) and loss (green arrows). Aphidicolin (APH)-treated cells were used as a positive control. % of fragile telomeres and telomere loss per metaphase are shown as violin plots. Data from two independent experiments are represented as median +/- first and third quartiles (grey dotted lines) (n≥45 metaphases). Student's t test ****, p <0.0001; ns, non-significant. Scale bar, 10 μm. (B) Flow cytometry analysis of the cell cycle distribution in shCONTROL and shSKIV2L HeLa cells untreated (DMSO) or aphidicolin treated (APH). DNA was stained with propidium iodide and cells were incubated with EdU to mark newly synthesised DNA. The percentage of cells in G1, early S phase (S1), late S phase (S2) and G2/M phases is indicated (n=10000 cells). Quantification of three independent experiments is shown, where data from S1 and S2 are merged as dataset S. Data are represented as mean +/- SEM. (C) WB analysis of ATR, pS345 CHK1, CHK1 (loading control), pS1981 ATM, ATM (loading control), pT68 CHK2 and CHK2 (loading control) in control and SKIV2L knockdown HeLa cells treated with DMSO (control) or aphidicolin. (D) Representative images of TRF2, S1981 ATM and 53BP1 IF staining in control and SKIV2L knockdown HeLa cells treated with DMSO (-) or aphidicolin (+). % of S1981 ATM or 53BP1 foci colocalising with TRF2 per cell are normalised to shCONTROL untreated samples and are represented as mean +/- SEM from three independent experiments. At least 100 cells were scored per experiment. Two-tailed student's t test *, p<0.05; **, p<0.01; ns, non-significant. Scale bar, 15 μm.

References

Alonso, C.R. (2005). Nonsense-mediated RNA decay: a molecular system micromanaging individual gene activities and suppressing genomic noise. Bioessays *27*, 463-466.

Aly, H.H., Suzuki, J., Watashi, K., Chayama, K., Hoshino, S., Hijikata, M., Kato, T., and Wakita, T. (2016). RNA Exosome Complex Regulates Stability of the Hepatitis B Virus X-mRNA Transcript in a Non-stop-mediated (NSD) RNA Quality Control Mechanism. J Biol Chem *291*, 15958-15974.

Arora, R., and Azzalin, C.M. (2015). Telomere elongation chooses TERRA ALTernatives. RNA Biol *12*, 938-941.

Arora, R., Lee, Y., Wischnewski, H., Brun, C.M., Schwarz, T., and Azzalin, C.M. (2014). RNaseH1 regulates TERRA-telomeric DNA hybrids and telomere maintenance in ALT tumour cells. Nat Commun *5*, 5220.

Azzalin, C.M., and Lingner, J. (2006). The human RNA surveillance factor UPF1 is required for S phase progression and genome stability. Curr Biol *16*, 433-439.

Azzalin, C.M., and Lingner, J. (2015). Telomere functions grounding on TERRA firma. Trends Cell Biol *25*, 29-36.
Azzalin, C.M., Reichenbach, P., Khoriauli, L., Giulotto, E., and Lingner, J. (2007). Telomeric repeat containing RNA and RNA surveillance factors at mammalian chromosome ends. Science *318*, 798-801.
Balk, B., Maicher, A., Dees, M., Klermund, J., Luke-Glaser, S., Bender, K., and Luke, B. (2013). Telomeric RNA-DNA hybrids affect telomere-length dynamics and senescence. Nat Struct Mol Biol *20*, 1199-1205.
Barroso, S., Herrera-Moyano, E., Munoz, S., Garcia-Rubio, M., Gomez-Gonzalez, B., and Aguilera, A. (2019). The DNA damage response acts as a safeguard against harmful DNA-RNA hybrids of different origins. EMBO Rep *20*, e47250.
Chawla, R., Redon, S., Raftopoulou, C., Wischnewski, H., Gagos, S., and Azzalin, C.M. (2011). Human UPF1 interacts with TPP1 and telomerase and sustains telomere leading-strand replication. Embo j *30*, 4047-4058.
Chen, C.Y., Gherzi, R., Ong, S.E., Chan, E.L., Raijmakers, R., Pruijn, G.J., Stoecklin, G., Moroni, C., Mann, M., and Karin, M. (2001). AU binding proteins recruit the exosome to degrade ARE-containing mRNAs. Cell *107*, 451-464.
Chu, H.P., Cifuentes-Rojas, C., Kesner, B., Aeby, E., Lee, H.G., Wei, C., Oh, H.J., Boukhali, M., Haas, W., and Lee, J.T. (2017). TERRA RNA Antagonizes ATRX and Protects Telomeres. Cell *170*, 86-101.e116.
Crossley, M.P., Bocek, M., and Cimprich, K.A. (2019). R-Loops as Cellular Regulators and Genomic Threats. Mol Cell *73*, 398-411.
Dejardin, J., and Kingston, R.E. (2009). Purification of proteins associated with specific genomic Loci. Cell *136*, 175-186.
Fairman-Williams, M.E., Guenther, U.P., and Jankowsky, E. (2010). SF1 and SF2 helicases: family matters. Curr Opin Struct Biol *20*, 313-324.
Flynn, R.L., Centore, R.C., O'Sullivan, R.J., Rai, R., Tse, A., Songyang, Z., Chang, S., Karlseder, J., and Zou, L. (2011). TERRA and hnRNPA1 orchestrate an RPA-to-POT1 switch on telomeric single-stranded DNA. Nature *471*, 532-536.
Garcia-Muse, T., and Aguilera, A. (2019). R Loops: From Physiological to Pathological Roles. Cell *179*, 604-618.
Garcia-Rubio, M., Barroso, S.I., and Aguilera, A. (2018). Detection of DNA-RNA Hybrids In Vivo. Methods Mol Biol *1672*, 347-361.
Graf, M., Bonetti, D., Lockhart, A., Serhal, K., Kellner, V., Maicher, A., Jolivet, P., Teixeira, M.T., and Luke, B. (2017). Telomere Length Determines TERRA and R-Loop Regulation through the Cell Cycle. Cell *170*, 72-85.e14.
Halbach, F., Reichelt, P., Rode, M., and Conti, E. (2013). The yeast ski complex: crystal structure and RNA channeling to the exosome complex. Cell *154*, 814-826.
Hockemeyer, D., Sfeir, A.J., Shay, J.W., Wright, W.E., and de Lange, T. (2005). POT1 protects telomeres from a transient DNA damage response and determines how human chromosomes end. Embo j *24*, 2667-2678.
Hug, N., Longman, D., and Caceres, J.F. (2016). Mechanism and regulation of the nonsense-mediated decay pathway. Nucleic Acids Res *44*, 1483-1495.
Isken, O., and Maquat, L.E. (2007). Quality control of eukaryotic mRNA: safeguarding cells from abnormal mRNA function. Genes Dev *21*, 1833-1856.
Lee, Y.W., Arora, R., Wischnewski, H., and Azzalin, C.M. (2018). TRF1 participates in chromosome end protection by averting TRF2-dependent telomeric R loops. Nat Struct Mol Biol *25*, 147-153.

Maicher, A., Kastner, L., Dees, M., and Luke, B. (2012). Deregulated telomere transcription causes replication-dependent telomere shortening and promotes cellular senescence. Nucleic Acids Res *40*, 6649-6659.
Mitchell, P., and Tollervey, D. (2003). An NMD pathway in yeast involving accelerated deadenylation and exosome-mediated 3'-->5' degradation. Mol Cell *11*, 1405-1413.
Nguyen, D., Grenier St-Sauveur, V., Bergeron, D., Dupuis-Sandoval, F., Scott, M.S., and Bachand, F. (2015). A Polyadenylation-Dependent 3' End Maturation Pathway Is Required for the Synthesis of the Human Telomerase RNA. Cell Rep *13*, 2244-2257.
Orban, T.I., and Izaurralde, E. (2005). Decay of mRNAs targeted by RISC requires XRN1, the Ski complex, and the exosome. Rna *11*, 459-469.
Ourliac-Garnier, I., and Londono-Vallejo, A. (2011). Telomere strand-specific length analysis by fluorescent in situ hybridization (Q-CO-FISH). Methods Mol Biol *735*, 33-46.
Petti, E., Buemi, V., Zappone, A., Schillaci, O., Broccia, P.V., Dinami, R., Matteoni, S., Benetti, R., and Schoeftner, S. (2019). SFPQ and NONO suppress RNA:DNA-hybrid-related telomere instability. Nat Commun *10*, 1001.
Pfeiffer, V., Crittin, J., Grolimund, L., and Lingner, J. (2013). The THO complex component Thp2 counteracts telomeric R-loops and telomere shortening. Embo j *32*, 2861-2871.
Porreca, R.M., Glousker, G., Awad, A., Matilla Fernandez, M.I., Gibaud, A., Naucke, C., Cohen, S.B., Bryan, T.M., Tzfati, Y., Draskovic, I.*, et al.* (2018). Human RTEL1 stabilizes long G-overhangs allowing telomerase-dependent over-extension. Nucleic Acids Res *46*, 4533-4545.
Porreca, R.M., Herrera-Moyano, E., Skourti, E., Law, P.P., Gonzalez Franco, R., Montoya, A., Faull, P., Kramer, H., and Vannier, J.B. (2020). TRF1 averts chromatin remodelling, recombination and replication dependent-break induced replication at mouse telomeres. Elife *9*.
Porro, A., Feuerhahn, S., Reichenbach, P., and Lingner, J. (2010). Molecular dissection of telomeric repeat-containing RNA biogenesis unveils the presence of distinct and multiple regulatory pathways. Mol Cell Biol *30*, 4808-4817.
Qu, X., Yang, Z., Zhang, S., Shen, L., Dangel, A.W., Hughes, J.H., Redman, K.L., Wu, L.C., and Yu, C.Y. (1998). The human DEVH-box protein Ski2w from the HLA is localized in nucleoli and ribosomes. Nucleic Acids Res *26*, 4068-4077.
Sagie, S., Toubiana, S., Hartono, S.R., Katzir, H., Tzur-Gilat, A., Havazelet, S., Francastel, C., Velasco, G., Chedin, F., and Selig, S. (2017). Telomeres in ICF syndrome cells are vulnerable to DNA damage due to elevated DNA:RNA hybrids. Nat Commun *8*, 14015.
Schmidt, C., Kowalinski, E., Shanmuganathan, V., Defenouillere, Q., Braunger, K., Heuer, A., Pech, M., Namane, A., Berninghausen, O., Fromont-Racine, M.*, et al.* (2016). The cryo-EM structure of a ribosome-Ski2-Ski3-Ski8 helicase complex. Science *354*, 1431-1433.
Sfeir, A., Kosiyatrakul, S.T., Hockemeyer, D., MacRae, S.L., Karlseder, J., Schildkraut, C.L., and de Lange, T. (2009). Mammalian telomeres resemble fragile sites and require TRF1 for efficient replication. Cell *138*, 90-103.
Silva, B., Pentz, R., Figueira, A.M., Arora, R., Lee, Y.W., Hodson, C., Wischnewski, H., Deans, A.J., and Azzalin, C.M. (2019). FANCM limits ALT activity by restricting telomeric replication stress induced by deregulated BLM and R-loops. Nat Commun *10*, 2253.

Singh, G., Jakob, S., Kleedehn, M.G., and Lykke-Andersen, J. (2007). Communication with the exon-junction complex and activation of nonsense-mediated decay by human Upf proteins occur in the cytoplasm. Mol Cell *27*, 780-792.
Stork, C.T., Bocek, M., Crossley, M.P., Sollier, J., Sanz, L.A., Chedin, F., Swigut, T., and Cimprich, K.A. (2016). Co-transcriptional R-loops are the main cause of estrogen-induced DNA damage. Elife *5*.
Takai, H., Smogorzewska, A., and de Lange, T. (2003). DNA damage foci at dysfunctional telomeres. Curr Biol *13*, 1549-1556.
Takai, K.K., Hooper, S., Blackwood, S., Gandhi, R., and de Lange, T. (2010). In vivo stoichiometry of shelterin components. J Biol Chem *285*, 1457-1467.
Taylor, L.L., Jackson, R.N., Rexhepaj, M., King, A.K., Lott, L.K., van Hoof, A., and Johnson, S.J. (2014). The Mtr4 ratchet helix and arch domain both function to promote RNA unwinding. Nucleic Acids Res *42*, 13861-13872.
Tseng, C.K., Wang, H.F., Burns, A.M., Schroeder, M.R., Gaspari, M., and Baumann, P. (2015). Human Telomerase RNA Processing and Quality Control. Cell Rep *13*, 2232-2243.
Tuck, A.C., Rankova, A., Arpat, A.B., Liechti, L.A., Hess, D., Iesmantavicius, V., Castelo-Szekely, V., Gatfield, D., and Buhler, M. (2020). Mammalian RNA Decay Pathways Are Highly Specialized and Widely Linked to Translation. Mol Cell *77*, 1222-1236.e1213.
van Hoof, A., Frischmeyer, P.A., Dietz, H.C., and Parker, R. (2002). Exosome-mediated recognition and degradation of mRNAs lacking a termination codon. Science *295*, 2262-2264.
Vannier, J.B., Pavicic-Kaltenbrunner, V., Petalcorin, M.I., Ding, H., and Boulton, S.J. (2012). RTEL1 dismantles T loops and counteracts telomeric G4-DNA to maintain telomere integrity. Cell *149*, 795-806.
Vannier, J.B., Sandhu, S., Petalcorin, M.I., Wu, X., Nabi, Z., Ding, H., and Boulton, S.J. (2013). RTEL1 is a replisome-associated helicase that promotes telomere and genome-wide replication. Science *342*, 239-242.
Wang, I.X., Grunseich, C., Fox, J., Burdick, J., Zhu, Z., Ravazian, N., Hafner, M., and Cheung, V.G. (2018). Human proteins that interact with RNA/DNA hybrids. Genome Res *28*, 1405-1414.
Wang, L., Lewis, M.S., and Johnson, A.W. (2005). Domain interactions within the Ski2/3/8 complex and between the Ski complex and Ski7p. Rna *11*, 1291-1302.
Wisniewski, J.R., Zougman, A., Nagaraj, N., and Mann, M. (2009). Universal sample preparation method for proteome analysis. Nat Methods *6*, 359-362.
Zinoviev, A., Ayupov, R.K., Abaeva, I.S., Hellen, C.U.T., and Pestova, T.V. (2020). Extraction of mRNA from Stalled Ribosomes by the Ski Complex. Mol Cell *77*, 1340-1349.e1346.

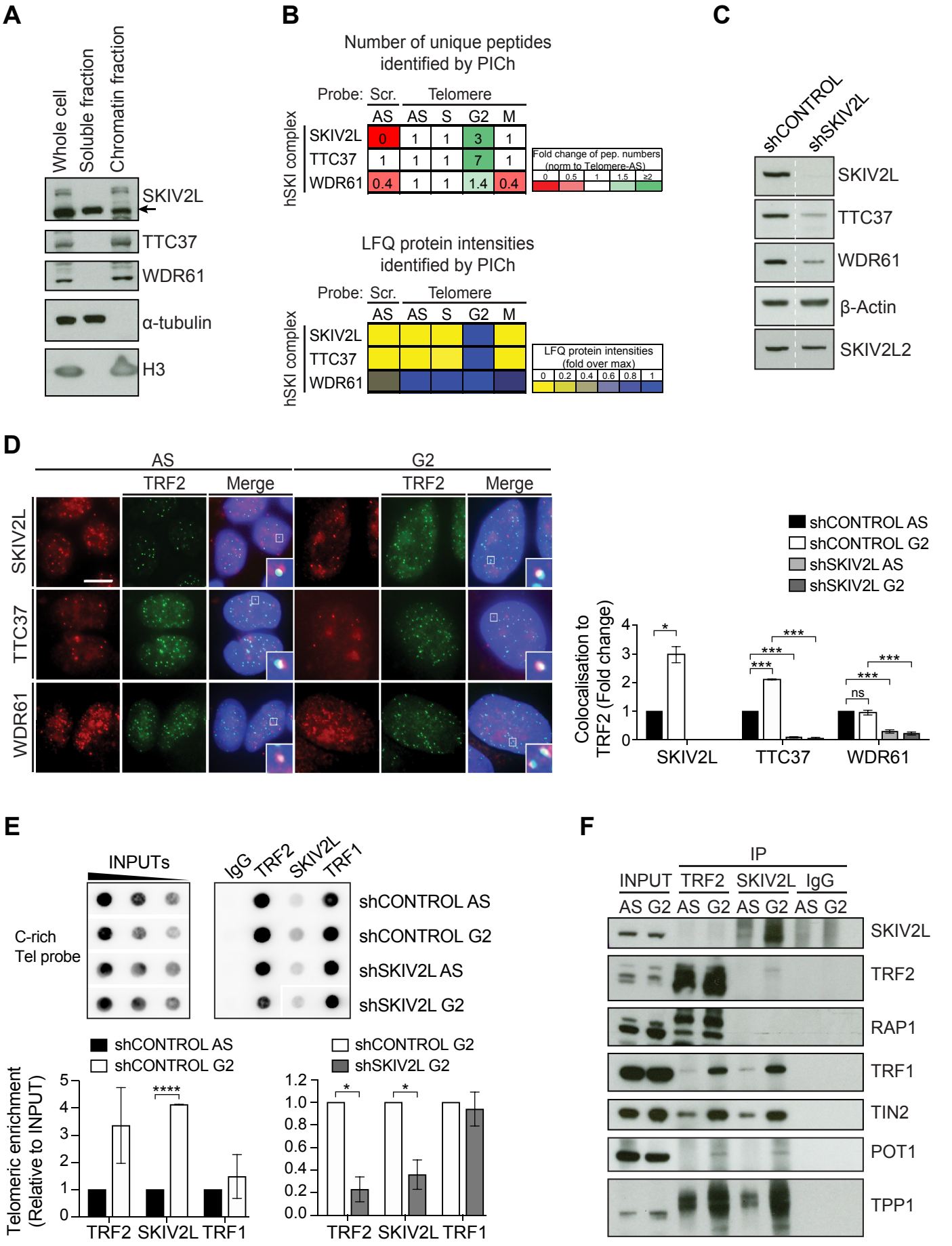
A
Whole cell
Soluble fraction
Chromatin fraction
SKIV2L
TTC37
WDR61
α-tubulin
H3
B
Number of unique peptides identified by PICh
Probe: Scr. Telomere
AS AS S G2 M
hSKI complex
SKIV2L 0 1 1 3 1
TTC37 1 1 1 7 1
WDR61 0.4 1 1 1.4 0.4
Fold change of pep. numbers (norm to Telomere-AS)
0 0.5 1 1.5 ≥2
LFQ protein intensities identified by PICh
Probe: Scr. Telomere
AS AS S G2 M
hSKI complex
SKIV2L
TTC37
WDR61
LFQ protein intensities (fold over max)
0 0.2 0.4 0.6 0.8 1
C
shCONTROL
shSKIV2L
SKIV2L
TTC37
WDR61
β-Actin
SKIV2L2
D
AS
G2
TRF2
Merge
TRF2
Merge
SKIV2L
TTC37
WDR61
shCONTROL AS
shCONTROL G2
shSKIV2L AS
shSKIV2L G2
Colocalisation to TRF2 (Fold change)
0 1 2 3 4
*
***
***
***
***
***
ns
SKIV2L
TTC37
WDR61
E
INPUTs
IgG
TRF2
SKIV2L
TRF1
C-rich Tel probe
shCONTROL AS
shCONTROL G2
shSKIV2L AS
shSKIV2L G2
shCONTROL AS
shCONTROL G2
Telomeric enrichment (Relative to INPUT)
0 1 2 3 4 5
****
TRF2 SKIV2L TRF1
shCONTROL G2
shSKIV2L G2
0.0 0.2 0.4 0.6 0.8 1.0 1.2
*
*
TRF2 SKIV2L TRF1
F
IP
INPUT TRF2 SKIV2L IgG
AS G2 AS G2 AS G2 AS G2
SKIV2L
TRF2
RAP1
TRF1
TIN2
POT1
TPP1

Fig. 1

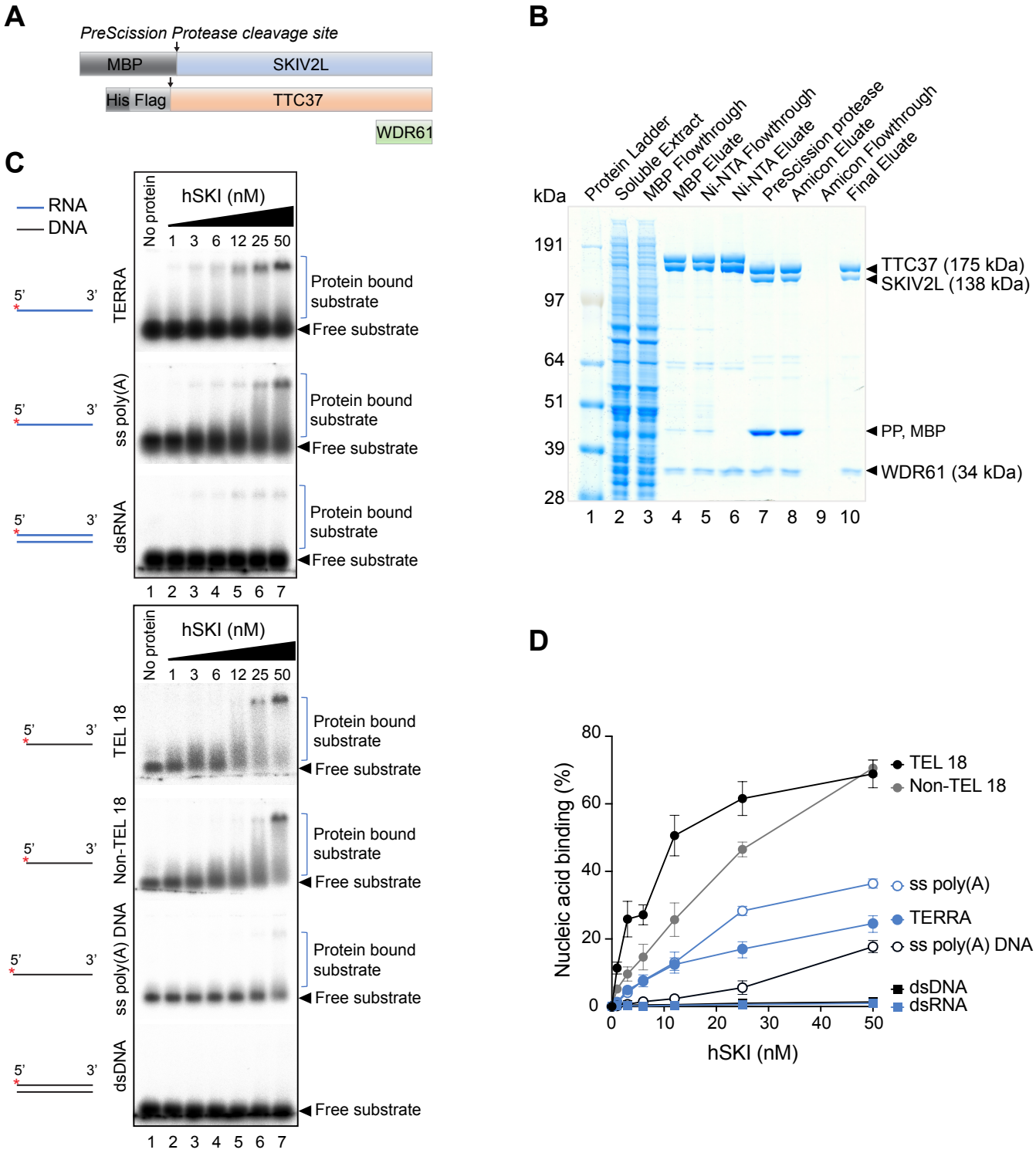
A
PreScission Protease cleavage site
MBP
SKIV2L
His Flag
TTC37
WDR61
B
kDa
Protein Ladder
Soluble Extract
MBP Flowthrough
MBP Eluate
Ni-NTA Flowthrough
Ni-NTA Eluate
PreScission protease
Amicon Eluate
Amicon Flowthrough
Final Eluate
191
97
64
51
39
28
TTC37 (175 kDa)
SKIV2L (138 kDa)
PP, MBP
WDR61 (34 kDa)
1 2 3 4 5 6 7 8 9 10
C
RNA
DNA
No protein
hSKI (nM)
1 3 6 12 25 50
TERRA
ss poly(A)
dsRNA
5' 3'
Protein bound substrate
Free substrate
1 2 3 4 5 6 7
TEL 18
Non-TEL 18
ss poly(A) DNA
dsDNA
D
Nucleic acid binding (%)
hSKI (nM)
TEL 18
Non-TEL 18
ss poly(A)
TERRA
ss poly(A) DNA
dsDNA
dsRNA

Fig. 2

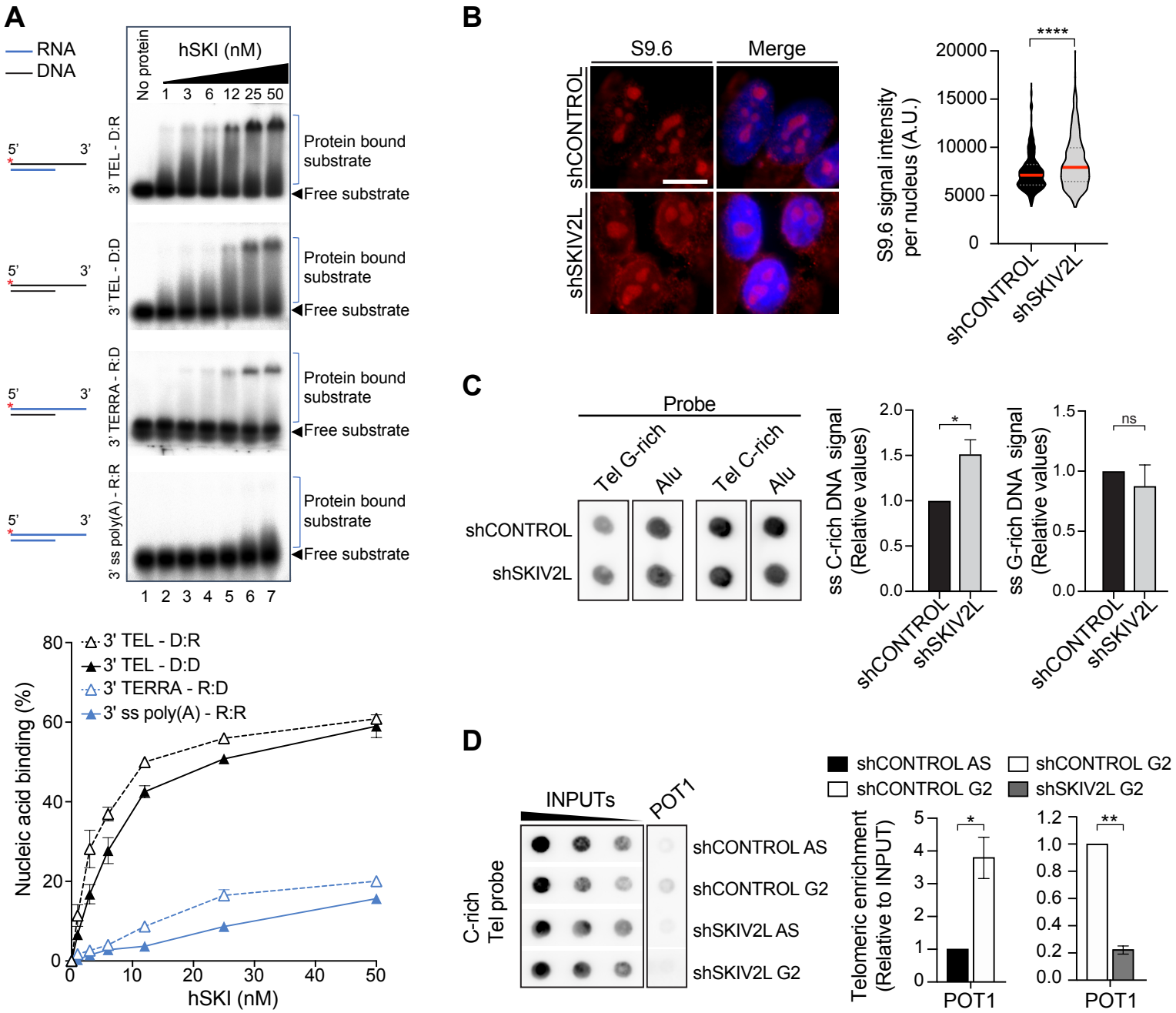
A
RNA
DNA
No protein
hSKI (nM)
1 3 6 12 25 50
5' 3'
3' TEL - D:R
3' TEL - D:D
3' TERRA - R:D
3' ss poly(A) - R:R
Protein bound substrate
Free substrate
1 2 3 4 5 6 7
Nucleic acid binding (%)
hSKI (nM)
B
S9.6
Merge
shCONTROL
shSKIV2L
S9.6 signal intensity per nucleus (A.U.)
****
C
Probe
Tel G-rich
Alu
Tel C-rich
ss C-rich DNA signal (Relative values)
ss G-rich DNA signal (Relative values)
*
ns
D
INPUTs
POT1
C-rich Tel probe
shCONTROL AS
shCONTROL G2
shSKIV2L AS
shSKIV2L G2
Telomeric enrichment (Relative to INPUT)
**

Fig. 3

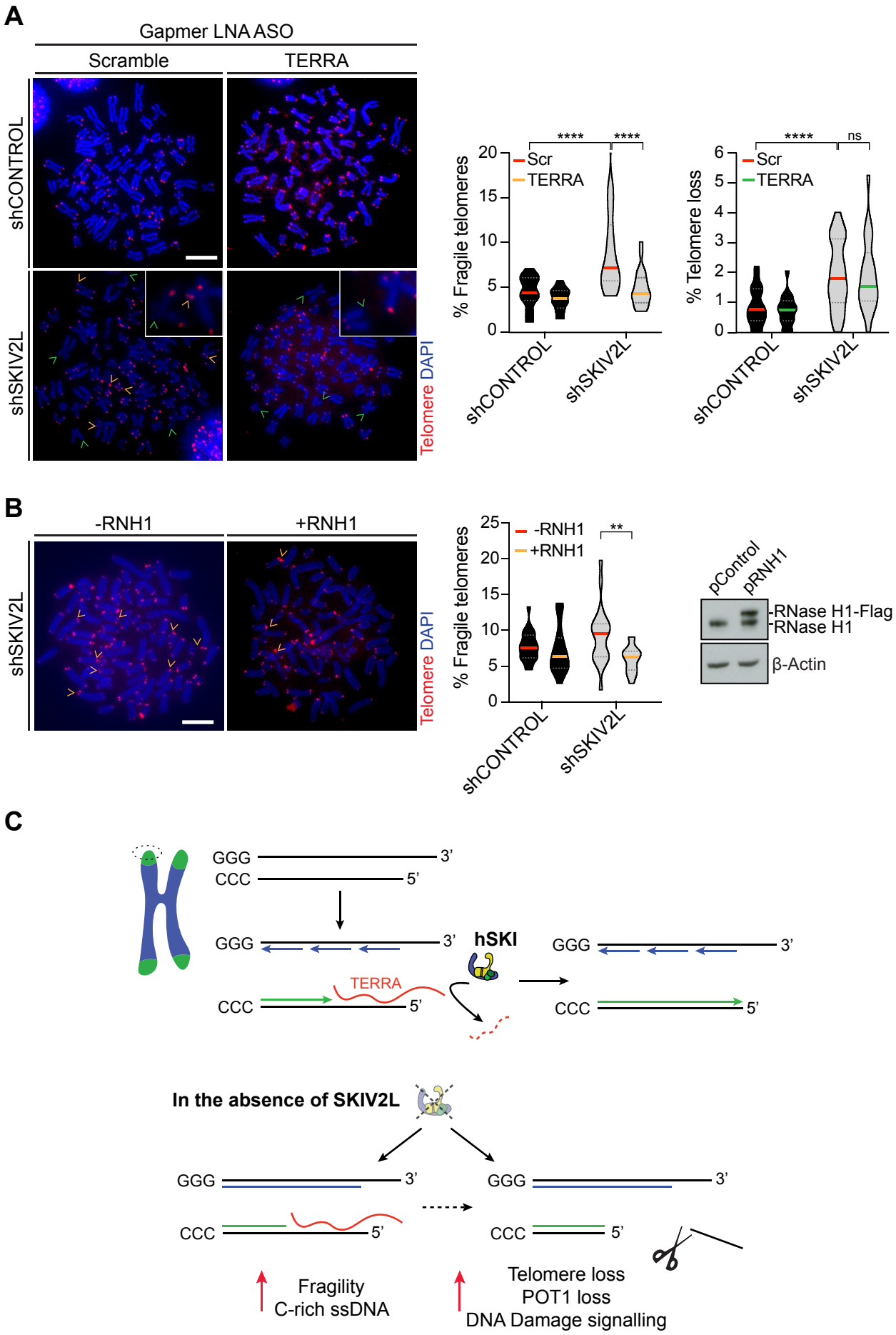
A
Gapmer LNA ASO
Scramble
TERRA
shCONTROL
shSKIV2L
Telomere DAPI
% Fragile telomeres
Scr
TERRA
****
****
shCONTROL
shSKIV2L
% Telomere loss
****
ns
B
-RNH1
+RNH1
shSKIV2L
Telomere DAPI
% Fragile telomeres
-RNH1
+RNH1
**
pControl
pRNH1
RNase H1-Flag
RNase H1
β-Actin
C
GGG
CCC
3'
5'
hSKI
TERRA
In the absence of SKIV2L
Fragility
C-rich ssDNA
Telomere loss
POT1 loss
DNA Damage signalling

Fig. 4

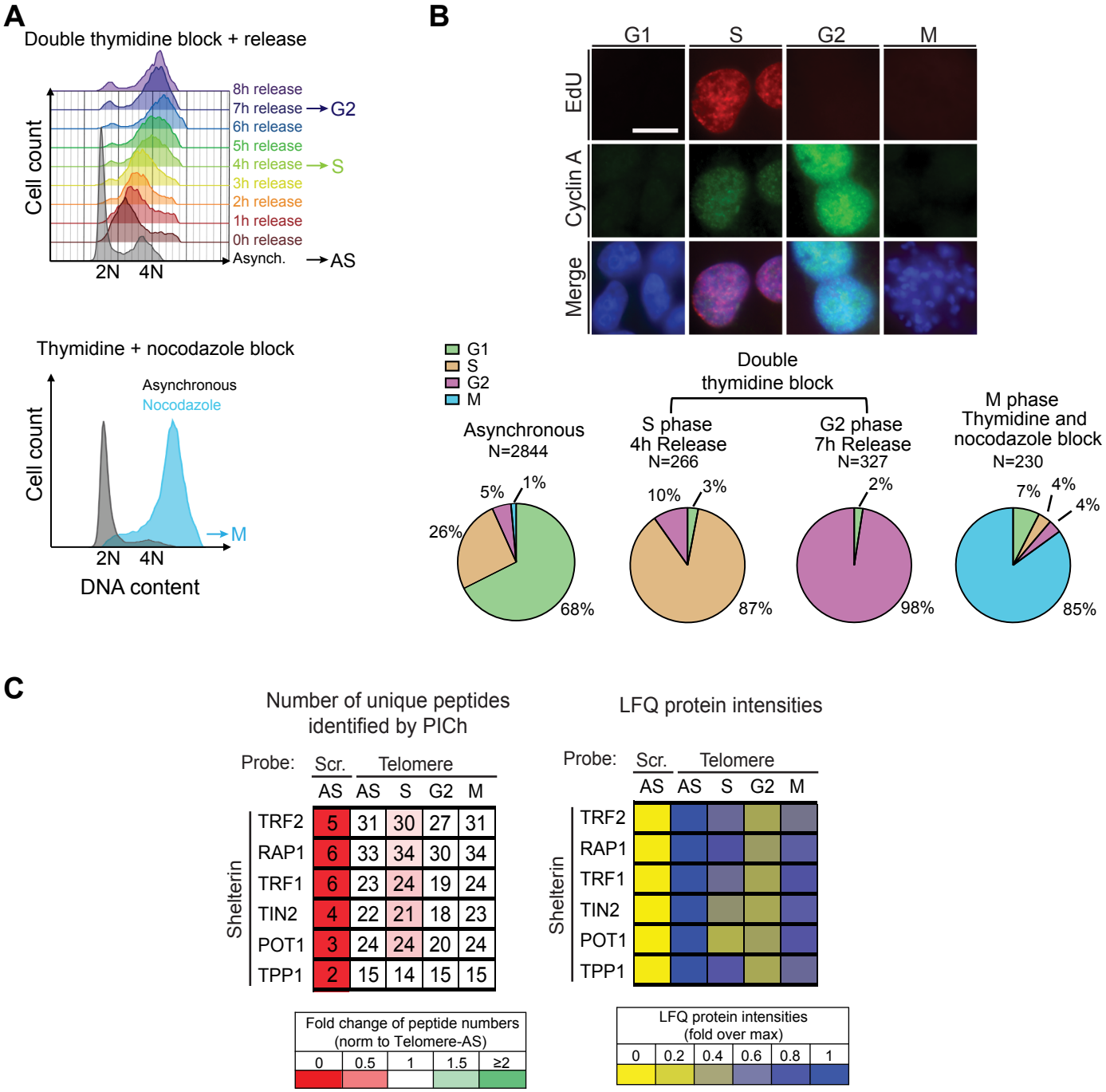
A
Double thymidine block + release
Cell count
8h release
7h release → G2
6h release
5h release
4h release → S
3h release
2h release
1h release
0h release
Asynch. → AS
2N 4N
Thymidine + nocodazole block
Asynchronous
Nocodazole
Cell count
→ M
2N 4N
DNA content
B
G1 S G2 M
EdU
Cyclin A
Merge
G1
S
G2
M
Double thymidine block
Asynchronous N=2844
S phase 4h Release N=266
G2 phase 7h Release N=327
M phase Thymidine and nocodazole block N=230
5% 1% 26% 68%
10% 3% 87%
2% 98%
7% 4% 4% 85%
C
Number of unique peptides identified by PICh
Probe: Scr. Telomere
AS AS S G2 M
Shelterin
TRF2 5 31 30 27 31
RAP1 6 33 34 30 34
TRF1 6 23 24 19 24
TIN2 4 22 21 18 23
POT1 3 24 24 20 24
TPP1 2 15 14 15 15
Fold change of peptide numbers (norm to Telomere-AS)
0 0.5 1 1.5 ≥2
LFQ protein intensities
Probe: Scr. Telomere
AS AS S G2 M
Shelterin
TRF2
RAP1
TRF1
TIN2
POT1
TPP1
LFQ protein intensities (fold over max)
0 0.2 0.4 0.6 0.8 1
D
shCONTROL
shSKIV2L
TRF2 Merge
TRF2 Merge
SKIV2L
TTC37
WDR61

Fig. S1

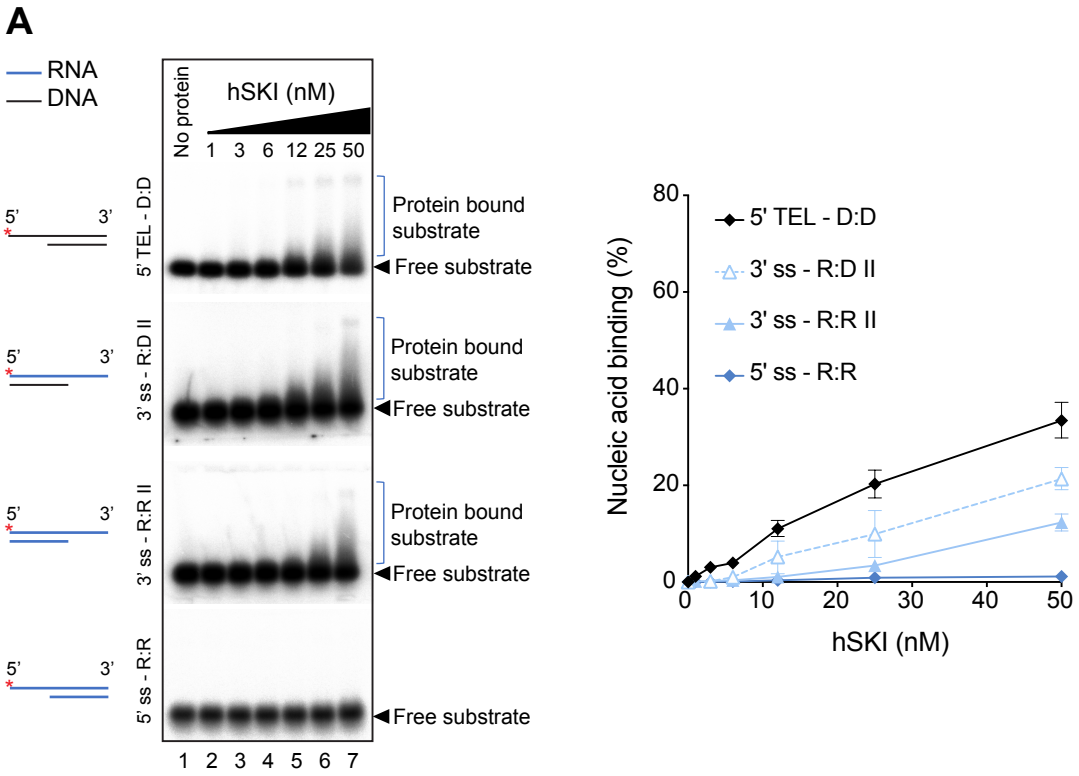
A
RNA
DNA
No protein
hSKI (nM)
1 3 6 12 25 50
5' TEL - D:D
3' ss - R:D II
3' ss - R:R II
5' ss - R:R
5'
3'
Protein bound substrate
Free substrate
1 2 3 4 5 6 7
Nucleic acid binding (%)
hSKI (nM)
0 10 20 30 40 50
0 20 40 60 80

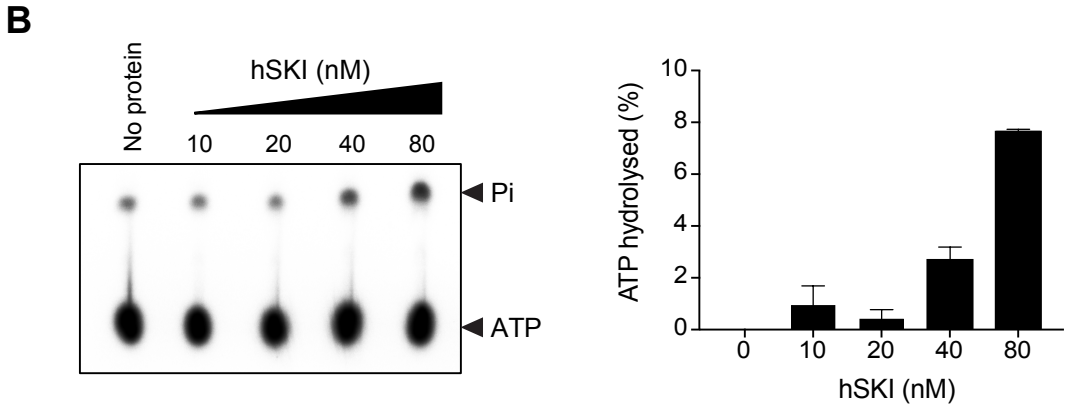
B
No protein
hSKI (nM)
10 20 40 80
Pi
ATP
ATP hydrolysed (%)
hSKI (nM)
0 10 20 40 80
0 2 4 6 8 10

Fig. S2

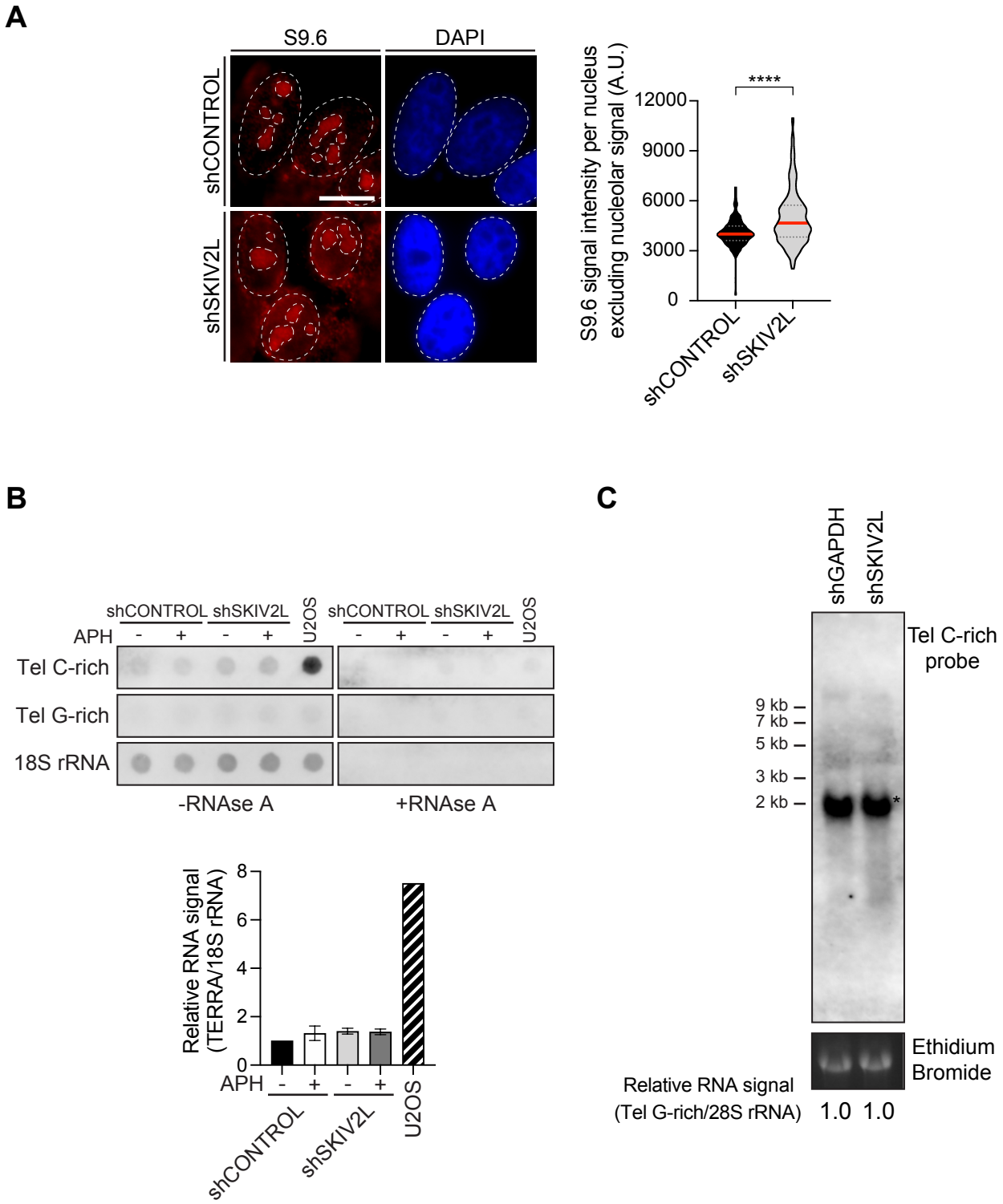
A
S9.6
DAPI
shCONTROL
shSKIV2L
S9.6 signal intensity per nucleus excluding nucleolar signal (A.U.)
****
12000
9000
6000
3000
0
shCONTROL
shSKIV2L
B
shCONTROL
shSKIV2L
U2OS
APH
Tel C-rich
Tel G-rich
18S rRNA
-RNAse A
+RNAse A
Relative RNA signal (TERRA/18S rRNA)
8
6
4
2
0
C
shGAPDH
shSKIV2L
Tel C-rich probe
9 kb
7 kb
5 kb
3 kb
2 kb
Ethidium Bromide
Relative RNA signal (Tel G-rich/28S rRNA)
1.0 1.0

Fig. S3

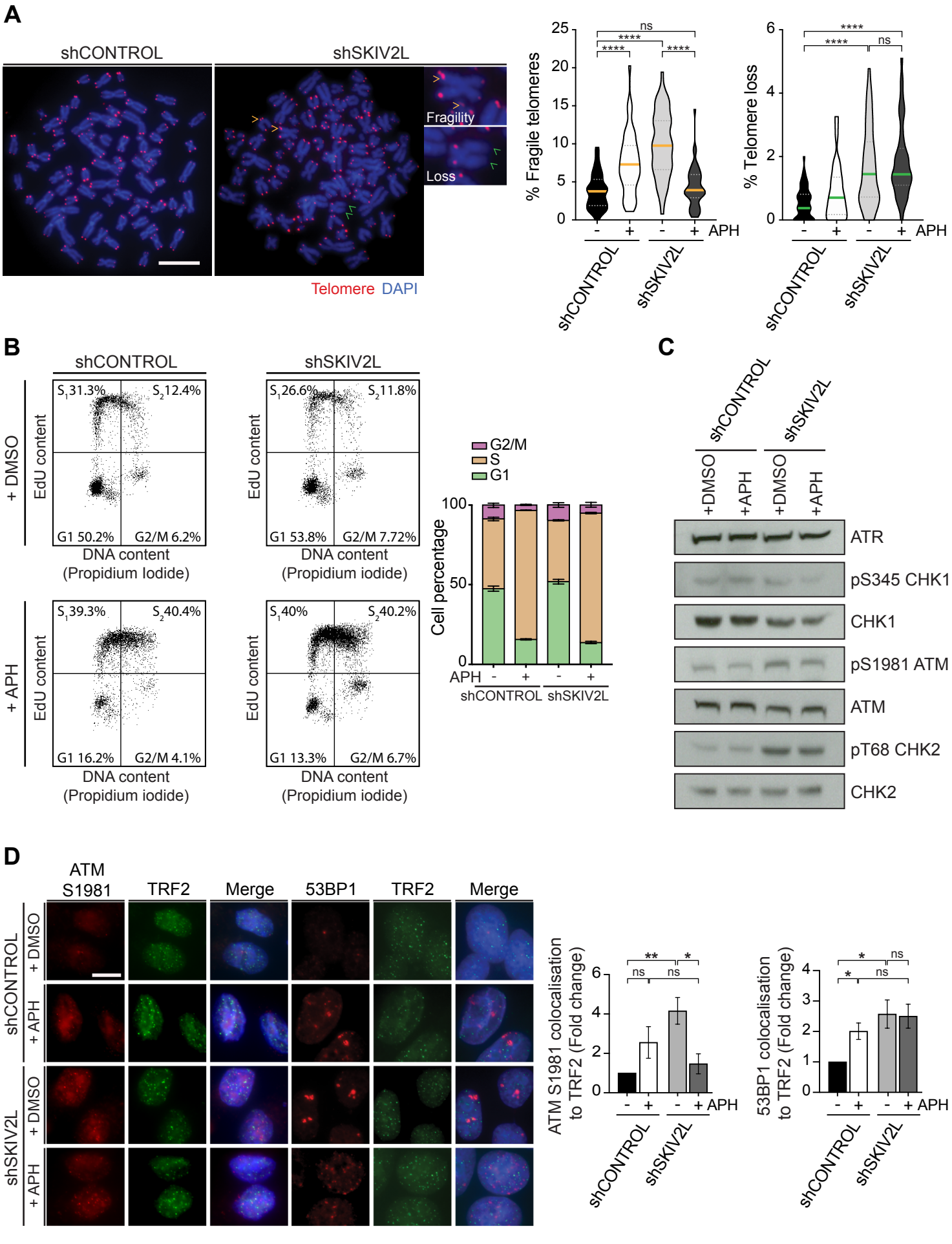
A
shCONTROL
shSKIV2L
Fragility
Loss
Telomere DAPI
% Fragile telomeres
% Telomere loss
APH
shCONTROL
shSKIV2L
B
shCONTROL
shSKIV2L
+ DMSO
+ APH
EdU content
DNA content
(Propidium Iodide)
(Propidium iodide)
G1 50.2%
G2/M 6.2%
G1 53.8%
G2/M 7.72%
G1 16.2%
G2/M 4.1%
G1 13.3%
G2/M 6.7%
G2/M
S
G1
Cell percentage
C
+DMSO
+APH
ATR
pS345 CHK1
CHK1
pS1981 ATM
ATM
pT68 CHK2
CHK2
D
ATM S1981
TRF2
Merge
53BP1
ATM S1981 colocalisation to TRF2 (Fold change)
53BP1 colocalisation to TRF2 (Fold change)

Fig. S4